Timed use of digoxin prevents heart ischemia-reperfusion injury through a REV-ERBα-UPS signaling pathway

Manjula Vinod, Alexandre Berthier, Xavier Maréchal, Céline Gheeraert, Raphaël Boutry, Stéphane Delhaye, Jean-Sébastien Annicotte, Hélène Duez, Agnès Hovasse, Sarah Cianférani, et al.

Timed use of digoxin prevents heart ischemia-reperfusion injury through a REV-ERBα-UPS signaling pathway

Manjula Vinod [1], Alexandre Berthier [1], Xavier Maréchal [1], Céline Gheeraert [1], Raphaël Boutry [2], Stéphane Delhaye [1], Jean-Sébastien Annicotte [2], Hélène Duez [1], Agnès Hovasse [3], Sarah Cianférani [3], David Montaigne [1], Jérôme Eeckhoute [1], Bart Staels [1], Philippe Lefebvre [1,*]

[1] Univ. Lille, Inserm, CHU Lille, Institut Pasteur de Lille, U1011-EGID, F-59000 Lille, France

[2] Univ. Lille, Inserm, CHU Lille, Institut Pasteur de Lille, U1167 – RID-AGE - Facteurs de risque et déterminants moléculaires des maladies liées au vieillissement, F-59000 Lille, France

[3] Laboratoire de Spectrométrie de Masse BioOrganique (LSMBO), IPHC, Université de Strasbourg, CNRS, UMR7178, 25 Rue Becquerel, F-67087 Strasbourg, France

[*] Corresponding author: philippe-claude.lefebvre@inserm.fr

UMR 1011, Bâtiment J&K, Faculté de Médecine de Lille-Pôle Recherche

Boulevard du Professeur Leclerc, 59045 Lille cedex, France

Tel +33.3.20974220

ABSTRACT

Myocardial ischemia-reperfusion injury (MIRI) induces life-threatening damages to the cardiac tissue and pharmacological means to achieve cardioprotection are sorely needed. MIRI severity varies along the day-night cycle and is molecularly linked to components of the cellular clock including the nuclear receptor REV-ERBα, a transcriptional repressor. Here we show that digoxin administration in mice is cardioprotective when timed to trigger REV-ERBα protein degradation. In cardiomyocytes, digoxin increases REV-ERBα ubiquitinylation and proteasomal degradation, which depend on REV-ERBα ability to bind its natural ligand, heme. Inhibition of the membrane-bound Src tyrosine-kinase partially alleviated digoxin-induced REV-ERBα degradation. In untreated cardiomyocytes, REV-ERBα proteolysis is controlled by several E3 ubiquitin ligases and the proteasome subunit PSMB5. Among these, only SIAH2 and PSMB5 contributed to digoxin-induced degradation of REV-ERBα. Thus, controlling REV-ERBα proteostasis through the ubiquitin-proteasome system is an appealing cardioprotective strategy. Our data support the timed use of clinically-approved cardiotonic steroids in prophylactic cardioprotection.

INTRODUCTION

The mammalian circadian clock is a critical cell-autonomous mechanism regulating many, if not all, aspects of cellular, tissular and organismal homeostasis [1]. Heart physiology makes no exception to this rule and electrophysiological, mechanical and metabolic functions of the cardiac tissue are submitted to cyclic daily variations [2], which are dependent on the integrity of the molecular clock [3]. Quite expectedly, genetic or environmental perturbations of the circadian clock in mouse models lead to cardiovascular pathologies including impaired cardiac contractility, fibrosis and cardiomyopathy. Human observational studies also largely concur to demonstrate that circadian rhythm misalignments are associated with cardiometabolic diseases [4]. The prevalence of adverse cardiovascular events such as stroke and myocardial infarction at the sleep-to-wake transition underlines the complex interplay between (mechanisms of) timed cyclic blood pressure control, heart function and vascular tone regulation. In addition to altering heart responsiveness to pathological events, circadian (dys)regulations also affect the heart and cardiomyocyte's ability to recover from acute injury.

Susceptibility to myocardial ischemia-reperfusion injury (MIRI) relies on transient adaptative mechanisms to hypoxia and rapid restoration of oxidative metabolism and contractile efficiency [5]. During ischemia, the myocardial tissue undergoes ATP depletion, acidosis by accumulation of lactic acid and activation of a series of immediate- and late- response intracellular signaling pathways called "RISK" and "SAFE" pathways. These signaling pathways, which are also stimulated upon preconditioning (PC), protect mitochondrial function [6]. Reperfusion causes massive cellular production of reactive oxygen species, alkalinization and calcium overload [7]. Sensitivity to MIRI is time-of-the-day (ToD)-dependent and is exacerbated during the sleep-to-wake transition in human and mouse [8]. Genetic alteration of circadian rhythmicity in mice [8] or circadian rhythm (dys)synchrony in humans correlate with increased acute cardiac injury [9]. We recently demonstrated that timed antagonism of the cyclically-expressed nuclear receptor REV-ERBα, a heme-binding transcriptional repressor within the molecular clock machinery, preventively protects mouse heart from deleterious effects of MIRI in a p21-dependent manner [10]. This observation mechanistically linked the ToD dependency of MIRI with the core clock gene machinery, identifying REV-ERBα as a novel target in pharmacological PC.

The search for pharmacologically protective compounds in MIRI has proven difficult [11]. Despite their continued use in atrial fibrillation to ameliorate heart contractile properties, cardiotonic steroids (CTS) such as digoxin are not recommended in MIRI cardioprotection at therapeutic concentrations [12]. Renewed interest in CTS has however sparkled from the identification of dissociated inotropic and non-ion pumping signaling properties of Na^+-K^+ ATPase (NKA), a target of CTS. Isoforms of the 3 NKA subunits [α, β and γ/FXYD] associate to make up the heteromeric membrane NKA complex Inotropic

effects of CTS are essentially mediated by their ability to bind to and inhibit NKA ATPase activity [13], thereby triggering intracellular accumulation of Na^+ and decreasing Ca^{++} efflux through the Na^+/Ca^{++} exchanger NCX1. CTS-induced signaling responses can be induced at ATPase sub-inhibitory concentrations and stems at least in part from NKA's ability to act as a CTS plasma membrane receptor [14,15]. CTS binding to the NKA α1 subunit allows the activation of multiple downstream intracellular signaling pathways, including part of RISK or SAFE pathways, hence suggesting a potential usefulness of CTS in preventive MIRI protection [16].

Thus, given the temporal gating of signaling pathways, the involvement of both the NKA signalosome and REV-ERBα in MIRI protection, and the known susceptibility of REV-ERBα activity to intracellular signaling pathways, we investigated whether CTS-induced signaling pathways could alter REV-ERBα functions and sensitivity to MIRI. Here we show that digoxin and other CTS activate signaling pathways in cardiomyocytes and trigger REV-ERBα protein degradation through the ubiquitin-proteasome system (UPS) in an SRC kinase-dependent manner. Timed in vivo treatment with digoxin prevented REV-ERBα protein accumulation and conferred protection against MIRI.

RESULTS

Cardioprotection by digoxin is time of the day-dependent.

We previously demonstrated, using the Langendorff heart perfusion model, that isolated mouse hearts display a ToD-dependent sensitivity to MIRI. Mouse hearts are intrinsically more resistant to MIRI at the beginning of the rest phase [zeitgeber time 0 (ZT0), beginning of the light phase] than at the end of this period (ZT12, average infarct size 27% vs 47%)([10] and Fig. 1a). We asked whether ex vivo PC efficiency follows a similar pattern. Submitting ZT0 isolated hearts to a short iterative ischemia-reperfusion sequence (PC) prior to a prolonged ischemic period neither protected nor aggravated infarct size. In contrast, MIRI-prone ZT12 hearts were protected by this local PC protocol (average infarct size 31% vs 47%) (Fig. 1a). To shed light on these differential sensitivities, the transcriptomic phenotype of ZT0 and ZT12 hearts was investigated (Fig. 1b and Supplementary Dataset 1). Only a few protein-encoding genes were found to be differentially expressed (n=145, Fig. 1b), with 10-12% being core circadian genes including REV-ERBα, which is lowest expressed at ZT0. In addition, ≈75% of differentially expressed genes are cyclically expressed with a period of 20-24 hours (Supplementary Dataset 1, Fig. 1b, right panel and Fig. 1c). None of them belonged to RISK or SAFE cardioprotective pathways. Thus, ZT12 hearts are intrinsically more sensitive to MIRI, responsive to PC and exhibit specific molecular phenotypic features related to molecular clock-driven processes.

We then assessed whether the previously reported ex vivo PC properties of digoxin can translate in vivo and whether they are ToD-dependent. We injected a single bolus of digoxin 4 hours prior to organ sampling at ZT0 or ZT9 at a pharmacologically well-tolerated dose (1 mpk IP [17]). This timing is based on pharmacokinetics studies of digoxin in rodents showing plasma concentration peaking within 1 hour after injection, followed by a 4- to 6-hour tissue distribution phase [18] yielding an estimated extracellular fluid concentration of about 5-10µM [19]. The infarct size in untreated mice was as in Fig. 1a, larger by 20% at ZT9 when compared to ZT0 hearts (Fig. 1d), in agreement with [10]. Whereas digoxin pretreatment showed a clear, albeit non-significant (p=0.08) trend to increase MIRI at ZT0, it significantly reduced infarct size by 20% at ZT9 (Fig. 1d). Pre-ischemic monitoring of heart performances with a constant flow perfusion did not reveal significant changes in contraction force, perfusion pression and myocardial contractility (Supplementary Fig. 1a-d), thus ruling out an effect of digoxin treatment on coronary vascular tone, endothelial function as well as on systolic and diastolic dynamics. In the MIRI model, a significant proportion of hearts displayed post-ischemic ventricular arrhythmias, making the analysis of cardiac contractile performance upon recovery infeasible.

Cardioprotection by digoxin is REV-ERBα-dependent.

Since the selected time points correspond to the nadir (ZT0) and zenith (ZT9) of REV-ERBα protein level, respectively (Fig. 1e and Extended data Fig. 1a), we assessed whether digoxin treatment affects REV-ERBα mRNA and protein levels. Increasing doses of digoxin administered at ZT5 led to a dose-dependent decrease REV-ERBα protein level at ZT9 to reach 60% at 1 mpk (Fig. 1f and Extended data Fig. 1b). In contrast, the expression of the REV-ERBα-encoding *Nr1d1* gene, whose expression precedes REV-ERBα protein expression by approximately 2 hours (Fig. 1c and Extended data Fig. 1c), was not affected by digoxin treatment. The expression of REV-ERBα target genes (*Arntl/Bmal1* and *Cdkn1a/p21,* Extended data Fig. 1c), which mirror the REV-ERBα protein level pattern in homeostatic conditions (Fig. 1c and Extended data Fig. 1c), were increased by digoxin treatment (Extended data Fig. 1d) as well as P21 protein levels (Extended data Fig. 1e). Digoxin did not affect REV-ERBα protein level at ZT0, which was barely detectable at this time point (Extended dataFig. 1f). This ToD sensitivity to digoxin was not due to changing levels during the day/night cycle of NKA isoforms *ATP1A1*, or *ATP1A2* and *ATP1A3* mRNAs or of corresponding protein levels at the time of treatment (Extended data Fig. 2a,b). Their expression was neither affected by REV-ERBα KO (Supplementary Dataset 2) nor by digoxin treatment (Extended data Fig. 2a). Thus, these data suggest that digoxin interferes with REV-ERBα protein levels through post-transcriptional regulation.

Digoxin administered at ZT4 did not protect mouse hearts from MIRI at ZT9 in *Nr1d1*$^{-/-}$ mice but rather increased infarct size (+11%) (Fig. 1g), phenotypically mimicking ZT0 hearts (Fig. 1d). REV-ERBα via p21 expression contributes to increased resistance to MIRI [10]. A similar experiment in p21-depleted mice confirmed the higher susceptibility of these mice to MIRI but digoxin treatment was still protective in these mice (-18%, average infarct size 55%)(Fig. 1g). Thus, REV-ERBα expression is required to confer cardioprotective properties to a prophylactic digoxin treatment without involving the anti-apoptotic protein P21.

Injected digoxin preferentially accumulates in skeletal muscles, heart and liver [20]. Similar to the cardiac tissue, digoxin-exposed livers displayed reduced REV-ERBα protein level and increased target gene expression (*E4bp4/Nfil3*, *Bmal1/Arntl*, *cdkn1a/p21*), while *Nr1d1* mRNA levels were left unchanged (Supplementary Fig. 2a-e). These observations raised the question of how digoxin downregulates REV-ERBα protein expression.

Digoxin affects REV-ERBα proteostasis in a cell-autonomous manner.

Analysis of bulk cardiac tissue as above may overlook outcomes stemming from multiple inter- or intracellular crosstalks. We therefore asked whether REV-ERBα protein degradation occurs in isolated digoxin-treated cardiomyocytes. We first performed experiments using the human cardiomyocyte cell line AC16 from adult human ventricular heart tissue [21]. Since digoxin and other CTS have significant pro-apoptotic properties [22], we investigated whether digoxin induces AC16 cell death. AC16 cells were synchronized at T_{-2} by a dexamethasone pulse (2 hours) which transiently induces *Per1* gene expression [23] and subsequently incubated with digoxin at T_0. Cell viability was only mildly affected by digoxin at tested concentrations (Extended data Fig. 3a). Probing apoptosis-related protein levels in AC16 whole cell extracts did not reveal any significant change in the apoptotic cascade (Extended data Fig. 3b). In these conditions, REV-ERBα reached a maximal expression 24 hours after synchronization (T_{24}). Digoxin blunted REV-ERBα expression at all time-points (Fig. 2a and Extended data Fig. 3c). REV-ERBα protein levels were normalized to HSP90α levels, whose half-life is 36-40 hours, vs 1 hour for REV-ERBα. NKA subunits α1 and α2 mRNAs and protein levels were steadily detectable in these conditions (Extended data Fig. 2c,d). Digoxin's effect on REV-ERBα protein level was fully prevented by an anti-digoxin antibody (Extended data Fig. 3d), excluding any artifactual modulation of cellular pathways by contaminants. The digoxin effect was dose-dependent with an observed EC_{50}= 96nM (Extended data Fig. 3e), which fits with the reported binding constant of digoxin to the human NKA α1 subunit (K_D=87nM), the major CTS signalosome relay [24,25]. It is also consistent with the observed efficiency of the non-glycosylated CTS bufalin [EC_{50}<0.1µM (Extended data Fig. 3f), K_D=42nM [24]]. The structurally-related ouabain also decreased REV-ERBα stability (Extended data Fig. 3g).

Under basal conditions, expression levels of *NR1D1* and of the REV-ERBα target gene *ANRTL/BMAL1* showed, as expected, an antiphasic transcript expression in untreated AC16 cells (Fig. 2b). Digoxin increased at T_{24} both *NR1D1* and *ANRTL/BMAL1* mRNAs, both known to be directly and cyclically repressed by REV-ERBα (Fig. 2b) and *ANRTL/BMAL1* promoter activity became acyclic (Fig. 2c). P21 protein level increased upon digoxin treatment (Fig. 2D), alike after in vivo digoxin injection (Extended data Fig. 1e).

Digoxin's effect was also assessed using the human osteosarcoma U2OS cell line, a commonly used and robust circadian model (Extended data Fig. 4a-c). REV-ERBα expression peaked 16-20 hours after synchronization, and digoxin blunted REV-ERBα protein level at all time-points (Extended data Fig. 4a). The expression of RORα, a transactivator counteracting REV-ERBα activity, remained unchanged (Extended data Fig. 4a) whereas *NR1D1* and BMAL*1/ARNTL* transcripts were higher expressed (Extended data Fig. 4b), with *ANRTL/BMAL1* promoter activity becoming acyclic (Extended data Fig. 4c). Similar results were obtained using human primary cardiomyocytes (Fig. 3) and HepG2

cells (Supplementary Fig. 2f). Thus, CTS strongly decrease REV-ERBα protein level in several representative cardiomyocyte models and unrelated cell lines (U2OS, HepG2), suggesting a highly conserved mechanism involving NKA.

Digoxin induces multiple intracellular signaling pathways.

Digoxin's effect on REV-ERBα levels are detected after a short treatment (210 minutes, Extended data Fig. 3h). Therefore, digoxin (at 5x EC_{50}=0.5µM) and other modulators were, in further experiments, added at T_{18}, 6 hours prior to the REV-ERBα protein peak in order to minimize secondary responses to treatment(s) (Fig. 4a, top panel). In these conditions, we assessed the involvement of NKA as a bifunctional protein regulating ion fluxes and exerting signaling functions, as the calculated in vivo concentration of digoxin (5-10µM, Fig. 1d) activates the signalosome-related PKCε in mouse heart [26]. In vitro, 3,4,5,6 tetrahydroxyxanthone (THX) inhibits NKA ATPase activity with an efficiency similar as ouabain (EC_{50}=1.6µM), while being unable to activate Src [27]**.** We therefore compared the activity of THX to that of digoxin on REV-ERBα stability. In contrast to digoxin, THX treatment did not alter REV-ERBα levels in AC16 (Fig. 4a and Supplementary Fig. 3a) and U2OS cells (Supplementary Fig. 3b), suggesting that the ion pumping activity of NKA is dispensable for digoxin-induced REV-ERBα decrease. Pharmacological perturbation of calcium fluxes through inhibition of voltage-dependent Ca^{++} channels by diltiazem and verapamil (Supplementary Fig. 3c), through SERCA inhibition by thapsigargin (Supplementary Fig. 3d) or through blockade of the Na^{+}-Ca^{++} exchange system NCX by KB-R7943 (Supplementary Fig. 3e) did not regulate REV-ERBα protein levels. Taken together, this data rules out a contribution of the inotropic arm of NKA.

The ability of digoxin to trigger intracellular pathways at low and moderate concentrations (0.5µM and 5.0µM) was thus evaluated using serine/threonine (S/T) kinase arrays (Fig. 4b-d). Digoxin activated multiple S/T kinases belonging mostly to the human CMGC (Cyclin-dependent kinases, Mitogen-activated protein kinases, Glycogen synthase kinases, CDC-like kinases), CAMK (Calcium and Calmodulin-regulated Kinases) and the related AGC (PKA, PKG, PKCs) groups (Fig. 4b-d). The IκB kinase complex was also detected as being significantly activated. Activation of representative kinases of the CMGC (ERK1&2) and the AGC (AKT1&2) groups was validated by an immunoblotting approach (Supplementary Fig. 4a,b). To disentangle downstream effects of digoxin-mediated signalosome activation, a genome-wide transcriptomic analysis was performed in similar conditions. As reported in other systems [28], digoxin increased the expression of immediate-early genes (IEGs) such as *EGR-1*, *c-FOS* and *c-JUN* both at low and high concentrations (Fig. 4e and Supplementary Dataset 3). Gene set enrichment analysis of upregulated genes identified the NFκB pathway as most robustly induced (Fig.

4f), in line with the phosphorylation of IκB kinase subunits (Fig. 4b, c). Monitoring gene expression in digoxin-exposed vs control mouse ZT9 hearts (Supplementary Dataset 4) showed an induction of *Egr-1*, *c-Fos* and *c-jun* and other immediate early genes, with a 31% (12/38) overlap (Fig. 3e, see *) between in vitro, digoxin-upregulated genes in AC16 cells and in vivo digoxin-upregulated genes in mouse heart.

Digoxin has been ascribed multiple effects owing to its ability to modulate the activity and/or expression of several proteins: it modulates transcriptional activity of the nuclear receptor RORγ [29], and interacts with PKM2 [30], a target gene of HIF1α whose translation is inhibited by digoxin [31]. Modulation of these pathways in AC16 cells by either a RORγ inverse agonist (ML209, Supplementary Fig. 5a), by knocking down *PKM2* (Supplementary Fig. 5b) or through *HIF1α* overexpression (Supplementary Fig. 5c) or activation (Supplementary Fig. 5d) did not blunt or exacerbate digoxin-induced REV-ERBα degradation. Thus, these 3 established digoxin targets are not effectors of digoxin action on REV-ERBα.

Thus, digoxin induces multiple signaling pathways, in murine cardiac tissue and cell lines, without engaging previously identified CTS targets. The causal link between digoxin-mediated induction of intracellular signaling pathways and altered REV-ERBα protein levels was further investigated.

The protein kinase SRC contributes to REV-ERBα stability.

We first pharmacologically modulated the known digoxin-sensitive SRC tyrosine kinase and the top-ranking digoxin-activated serine/threonine kinases identified above. We employed, in conjunction or not with digoxin, widely-used chemical modulators for SRC (PP2), PI_3K (ZSTK474), ERK1&2 (SCH772984), AKTs (MK2206), CAMK1&2 (KN93), MEK1&2 (PD98059), PKG1&2 (RP8-pCPT-cGMPS), PKD (CRT0066101), p70S6K1 (PF-4708671), RSK1&2&3 (BRD7389) and for components of the NFκB pathway such as LUBAC (Bay11-7082), HOIP (HOIPIN-8), IKKα/β (BMS345541), IKKβ (TCPA-1), IKKε and TBK1 (amlexanox) (Fig. 5 and Extended data Fig. 5). This approach proved highly efficient at inhibiting kinase activity (see Supplementary Fig. 4c as an example). Results were subsequently validated for a number of targets using either overexpressed constitutively active kinase mutants, other inhibitors or siRNAs (Extended data Fig. 6,7).

Stabilizing effects on basal REV-ERBα levels were observed when inhibiting PI3K, ERKs or MEKs (Fig. 5). However, this was not confirmed using distinct inhibitors or siRNAs with the exception of PI3K (Extended data Fig. 6). The latter effect was however not detected in U2OS cells (Supplementary Fig.

6a). Taken together, these data show that functional interference with this set of kinases did not significantly affect REV-ERBα stability in basal conditions.

Blunting ERKs, PI3K, AKTs, CAMKs, MEKs, PKGs, PKD1, P70S6K1, RSKs, IKKs or TBK activity did not impair digoxin's ability to trigger REV-ERBα degradation, a conclusion validated through the use of alternative approaches (Extended data Fig. 6,7). In contrast, inhibition of SRC (with PP2, Fig. 5a and with saracatinib, Extended data Fig. 6a, 7a) blunted digoxin-induced REV-ERBα protein decrease, an effect which, albeit less pronounced, was also observed in U2OS cells (Supplementary Fig. 6a). This data nevertheless suggested the involvement of SRC in the chain of events leading to decreased REV-ERBα levels.

Bay 11-7082 efficiently stabilized REV-ERBα in non-challenged cells and significantly protected REV-ERBα from digoxin-induced decreased expression in AC16 (Fig. 5j and Extended data Fig. 5j) and U2OS cells (Supplementary Fig. 13b). Initially described as a linear ubiquitin chain assembly complex (LUBAC) inhibitor, this compound also significantly inhibit several E2 ligases and the proteasome [32]. The use of a more specific inhibitor of the LUBAC complex, HOIPIN-8 [33] (Fig. 5k and Extended data Fig. 5k), of a *HOIL*-targeting siRNA (Extended data Fig. 6j, 7j) and the overexpression of the OUT domain-containing deubiquitinase with linear linkage specificity (OTULIN, Extended data Fig. 6k, 7k) show no significant effects in our assay, thereby excluding the LUBAC complex as contributing to the REV-ERBα degradation process.

Since the NFκB pathway was activated upon digoxin treatment, we assessed the involvement of this transcription factor in several ways. We first **searched for** a transcriptomic blueprint of the activated NFκB pathway in cardiac tissues from *Nr1d1*$^{-/-}$**mice**. A comparative analysis of *Nr1d1*$^{-/-}$ vs *Nr1d1*$^{+/+}$ heart transcriptome at ZT12 evidenced, alike the ZT0 vs ZT12 comparison (Fig. 1b,c), strong dysregulation of clock-related processes without any significant enrichment in NFκB-driven responses (Supplementary Fig. 7a). Up- and downregulated genes were searched against the EnrichR ChEA database to identify transcription factors binding in the vicinity of their promoters, on the basis of aggregated ChIP-seq studies [34]. This analysis did not identify NFκB as a potential regulator of dysregulated genes (Supplementary Fig. 7b). Overexpressing inhibitory wild type or super repressor (SR) IκBα [35] did not protect or enhance digoxin's effect on REV-ERBα stability (Supplementary Fig. 7c). Finally, the pharmacological NFκB modulator betulinic acid did not prevent the effect of digoxin on REV-ERBα protein levels, definitively excluding this pathway as a player in the observed REV-ERBα degradation (Supplementary Fig. 7d).

Our results thus show that SRC kinase, described as part of the digoxin-controlled "NKA signalosome", contributes to the observed decrease in REV-ERBα protein levels in AC16 and U2OS cells.

Bay 11-7082, which inhibits IκBα, E2 ligases Ubc13 and UbcH7, the E3 ligase LUBAC and the proteasome exerts a potent activity in our system, the effect of which being unrelated to the inhibition of linear ubiquitinylation by the LUBAC complex. These results rather pointed to the involvement of UPS in REV-ERBα degradation.

Digoxin induces the proteasomal degradation of REV-ERBα.

The UPS and autophagy are 2 main branches of the protein quality control pathway. Preliminary investigations ruled out other branches involving protein neddylation (using the NEDD8 inhibitor MLN4924/pevonedistat) or sumoylation (using the SUMO inhibitor 2-D08) as controlling REV-ERBα stability (Supplementary Fig. 8). The autophagy pathway was not modulated by digoxin (Supplementary Fig. 9a), contrasting with reports in cancerous cells 28557 [36]. Accordingly, pharmacological modulation of autophagy by either chloroquine, bafilomycin or rapamycin did not impact digoxin-induced effects (Supplementary Fig. 9b-d). Knocking down *P62/SQSTM1* expression, which was the sole component of the autophagy pathway upregulated by digoxin (Supplementary Fig. 9a), had no effect (Supplementary Fig. 9e).

We then explored if the UPS is implicated in digoxin-induced REV-ERBα degradation. The proteasome catalytic subunit beta 5 (PSBM5) inhibitors bortezomib (BTZ) and clasto-lactacystin β-lactone, albeit to a lesser extent, protected REV-ERBα from digoxin-induced degradation (Fig. 6a,b and Extended data Fig. 8a,b). Protection by BTZ was also observed in U2OS cells (Extended data Fig. 8c), suggesting that UPS is a conserved component of the REV-ERBα degradation pathway. As exogenously-expressed wild type REV-ERBα is equally sensitive to digoxin treatment (Fig. 6d and Extended data Fig. 8d), we assessed whether REV-ERBα undergoes ubiquitinylation and is modified upon digoxin treatment using overexpressed Flag-REV-ERBα in AC16 cells. Mono-, multi- and poly-ubiquitinylated proteins were isolated from whole cell extracts and REV-ERBα content was analyzed by western blot analysis. REV-ERBα was eluted along with other mono- and poly-ubiquitinated proteins, and its concentration decreased in digoxin-exposed cellular extracts, and increased in BTZ+digoxin-treated cells (Fig. 6e), indicative of a digoxin-controlled REV-ERBα ubiquitinylation. The H602F REV-ERBα mutant, which is unable to bind its natural ligand heme [37], showed higher expression in basal conditions as reported [38] and was digoxin-resistant (Fig. 6d and Extended data Fig. 8d), suggesting that heme binding to REV-ERBα promotes a conformation required for proteasomal degradation.

To determine which component(s) of the UPS pathway could be involved in REV-ERBα degradation, we isolated REV-ERBα interacting partners by RIME (rapid immunoprecipitation followed

by mass spectrometry identification of endogenous proteins) [39] using the digoxin-sensitive U2OS and HepG2 cells. We then filtered the generated list of interactors against the Gene Ontology "cellular component" or "molecular functions" databases using "proteasome" or "ubiquitin" as biological terms and interacting significantly with REV-ERBα (Supplementary Dataset 6). We identified 16 UPS-related proteins interacting with REV-ERBα, including several E2 (UBE2L3) and E3 (PRPF19, TRIM21) ubiquitin ligases, the NCoR complex component TBL1XR1, and 4 subunits of the proteasome (PSMA4, PSMA5, PSME3, PSMD2) (Fig. 7a). To this list of proteins potentially funneling REV-ERBα towards proteasomal degradation, we added a number of E2 and E3/E4 ubiquitin ligases previously reported to regulate REV-ERBα protein stability (SIAH2 [40], FBWX7 [41], HUWE1 [42]) or predicted to act on REV-ERBα using the proteome-wide E3 ligases-substrate interaction network (UbiBrowser [43]) such as BRCA1, CBL, MDM2, STUB1, TRIM33 and the ubiquitination factors UBE4A and UBE4B. The final list totaled 28 proteins (Fig. 7b), from which 19 were tested for their involvement in REV-ERBα degradation. AC16 cells were thus transfected with siRNAs or treated with pharmacological inhibitors when available. Results are summarized (Fig. 7) from the quantification (Extended data Fig. 9) of raw data (Extended data Fig. 10). NEDD8, PSME3, the FBXW7-dependent destabilizing kinase CDK1 [41], the REV-ERBα stabilizing kinase GSK3β [44], BRCA1, UBE4A, MDM2, STUB1 and TRIM33 were inactive in our assay (Extended data Fig. 9). Six entities significantly contributed to REV-ERBα stability in basal conditions including the REV-ERBα-interacting, NCoR complex component TBL1XR1 and the E3 ligases SIAH2, HUWE1, FBXW7, CBL and UBE4B. Quite unexpectedly, impaired expression of the E2 ligase-encoding gene *UBE2L3/UBCH7* decreased basal REV-ERBα expression (Extended data Fig. 9d). However, none of these E3 ligases modulated the digoxin-mediated REV-ERBα degradation, with the exception of SIAH2, whose knockdown partially maintained REV-ERBα level (Extended data Fig. 9a). Thus, digoxin-mediated activation of UPS triggers REV-ERBα degradation through a complex chain of events yet to be identified, but including the E3 ligase SIAH2 and the proteasome subunit PSMB5 (Fig. 8).

DISCUSSION

In the current era of precision medicine wherein therapies are formulated and administered to attain maximal benefit through increased efficiency and reduced side effects, chronotherapy is an important step further towards this goal. As an edifying example, chrono-chemotherapy is beneficial in combating cancer by using a circadian window of higher drug tolerability and efficiency [45]. Chronotherapy has been recently extended to hypertension treatment at bedtime, and proved more efficient at decreasing CVD events [46].

The unevenly distributed rate of occurrence of cardiac events suggest a differential sensitivity of the heart to injury along the 24h day-night period [8]. ToD dependent functional variations occur in heart physiology, which are partly reflected by the significantly oscillating expression of approximately 13% of cardiac genes, which are involved in multiple functions from signaling and growth to transcription and cardiac remodeling [3,47]. Similarly, proteomic analysis established striking differences in night versus day protein levels in heart [48], suggesting that timed cardiac proteostasis is crucial to proper heart function. Along these lines, we reported a strong correlation between the time of surgery and perioperative myocardial tolerance to injury in patients undergoing aortic valve replacement. This ToD-dependent differential myocardial sensitivity to IRI was attributed to the rhythmic expression of the nuclear receptor REV-ERBα and of its anti-apoptotic target gene *P21* [10]. We also suggested the therapeutic potential of pharmacological inhibition of REV-ERBα for prophylactic cardioprotection. This provided an alternative approach to physical ischemic PC in which multiple distal, brief ischemic episodes induce cardioprotective signaling pathways that bestow protection in a future event of prolonged ischemia.

With the realization that NKA, the primary target of digoxin and other CTS, controls the activation of multiple signaling pathways including part of the RISK and SAFE pathways such as AKT, PKC and tyrosine kinases (Fig. 4), the use of CTS as PC agents has been proposed [16]. Cardioprotection is observed in rats dosed with a sub-ionotropic dose of ouabain followed by washout similarly to IPC [25,49]. However, this strategy has not yet gained momentum, as digoxin use in heart failure and atrial fibrillation has stirred a 200-year long history of controversies, leading to clinical hesitancy to widen digoxin and other CTS use in PC and other pathologies [50-52].

Our study however demonstrates a ToD-dependent action of digoxin on myocardial integrity. The decreased susceptibility to IRI in mice dosed with digoxin when REV-ERBα expression reaches its maximum (ZT9) could be potentially attributed to 2 principal effects: (1) circadian rhythm alteration and/or (2) pharmacological cardiac preconditioning through the rapid and potent activation of many components of the RISK and SAFE pathway including PI3K, AKT, ERK1/2, GSK3β, and NFκB (Fig. 3).

Genetic ablation of REV-ERBα showed that its expression is mandatory to observe digoxin protective effects. Digoxin treatment in mice relieved REV-ERBα repression on several genes including the cardioprotective *Bmal1* and *cdkn1a* (Extended data Fig. 1 and Supplementary Dataset 4). The anti-apoptotic P21 is not required for the cardioprotective effect of digoxin. Cardioprotective activities of BMAL1 have been elegantly documented through the use of genetic models [53]. The ZT12-digoxin phenotype is reminiscent of that of CCM mice, whose clock is locked at the wake-to-sleep transition (ZT0), display improved tolerance to MIRI at ZT12 and in which *Bmal1* is similarly upregulated with dampened cyclicity [8]. Identified BMAL1 target genes include *Nampt* or *Coq10b* which replenish cellular stores in cardioprotective NAD^+ and ubiquinone respectively [54]. However, digoxin-exposed hearts displayed no altered expression of these and other BMAL1 target genes (Supplementary Dataset 4), an outcome likely due to the short time frame (4 hours) of the acute digoxin treatment. Thus, BMAL1 is unlikely to play a role in the observed phenomenon.

In contrast to these cardioprotective effects at ZT9, digoxin treatment of REV-ERBα-depleted hearts (ZT0) resulted in, albeit non-significant, trend to increased susceptibility to MIRI. As our transcriptomic studies did not point to obvious mechanisms, the molecular basis for this differential sensitivity to digoxin at ZT0 is unclear at this stage. Multiple parameters not assessible by gene expression studies may indeed control heart sensitivity to MIRI. Circadian variations of heart metabolism and temporal gating of signaling pathways may contribute to this time-specific response [53], while NKA α1 expression is constant throughout the day-night cycle (Extended data Fig. 2 and [55]). Alternatively, the subcellular localization of NKA subunits, which is exquisitely regulated and dependent on protein-protein interactions, may vary and affect it signaling properties.

An unexpected, yet one of the most important findings in our study is the impact of digoxin on REV-ERBα protein levels in vivo and in human primary and immortalized cardiomyocytes. Exogenously overexpressed REV-ERBα was found to be equally sensitive to digoxin and a target for the ubiquitination machinery. . In contrast, the overexpressed ligand binding-crippled H602F REV-ERBα mutant was resistant to digoxin-induced degradation. Thus, heme-binding to REV-ERBα, which may induce specific conformational changes in the aporeceptor structure, seems to be an important prerequisite for physiological ([56,57] and Fig. 6d) and digoxin-triggered degradation through the proteasomal pathway. Interestingly, heme regulatory motif (HRM)- or PAS (PER-ARNT-Sim)-containing transcription factors and clock components such as NPAS2, CLOCK, PER1 and PER2 are also subjected to heme-dependent protein degradation [58,59,60], linking heme synthesis and circadian rhythm regulation.

Our data thus clearly point to a beneficial effect of acute REV-ERBα antagonism in cardioprotection. This observation seems at odds with investigations reporting improvement of failing hearts 1-day post-MI following treatment with SR9009, a REV-ERB agonist [61], which induces cardiac transcriptomic alterations [62,63], and blockade of cardiac remodeling through an anti-inflammatory mechanism [64]. However, prolonged agonist treatment decreases, through a negative auto-feedback loop, REV-ERBα protein level [61]. Alternatively, it also triggers systemic immune cell mobilization [65], a process unlikely to be at play in our acute system.

CTS-controlled protein degradation is not unprecedented. Ouabain and digoxin triggers the degradation of the nuclear estrogen receptor ERα in primary and metastatic breast cancer cells, providing an additional mechanism for the reported CTS cytotoxicity against cancer cells [66]. Bufalin, which also induces REV-ERBα degradation (Extended data Fig. 3f), strongly impacts on p160 steroid receptor coactivator SRC1 and SRC3 protein stability [67]. Knockdown experiments however ruled out a contribution of SRC1 and 3 in our system (Supplementary Fig. 10). The pleotropic effects of CTS thus call for a careful examination of their side-effects. However, their use in cardiac PC as a timed, single, low dose administration is an appealing therapeutic strategy to improve patient outcome, as unwanted effects of these FDA-approved drugs will be predictably limited. On the contrary, prolonged exposure to CTS in either CVD or cancer therapy might impinge on the molecular clock in several organs including the liver (Supplementary Fig. 2), inducing metabolic alterations with unpredictable outcomes. Alternative approaches may be considered to target REV-ERBα for elimination. Combining REV-ERBα ligands to an E3 recognition motif to generate a PROteolysis TArgeting Chimera (PROTAC) may be an innovative strategy to lessen heart susceptibility to MIRI.

METHODS

Reagents

All information about reagents, chemicals, siRNAs, Taqman probes, antibodies, plasmids, transfection reagents, kits and softwares are provided in the accompanying Supplementary Information file.

Animal Experimentation

All experiments were approved by the Comité d'Ethique en Expérimentation Animale du Nord-Pas de Calais CEEA75. To eliminate sex as a confounder, male mice were used throughout this study. C57BL6/J wild-type male mice (10-14 weeks) were purchased from Charles River Laboratories and housed in a temperature-controlled environment (23-25°C, 40-60% humidity) with a 12h/12h light-dark cycle, ZT0 being lights-on. Mice had free access to water and were fed ad libitum a standard chow diet (Safe Diet A04). *Cdkn1a/p21*$^{-/-}$mice and their wild-type littermates were obtained from Charles River (France, B6. 129.S6(Cg)-Cdkn1atm1Led/J - SN 16565), *Nr1d1*$^{-/-}$ mice (SV129.*Nr1d1*$^{-/-}$ [68]) were bred, housed and fed as above.

To study the impact of digoxin in vivo, animals were injected intraperitoneally with digoxin or vehicle (10% ethanol, 40% propylene glycol, 0.08% citric acid, 0.3% sodium phosphate) at ZT5 or ZT20 at indicated concentrations (in most cases 1 mpk). The investigator was blinded to the treatment. Mice were sacrificed by cervical dislocation at ZT9 or ZT0. Organs were harvested and snap-frozen for protein and RNA analysis. Heart sensitivity to MIRI was tested using the ex vivo Langendorff perfused mouse heart model [69]. Isolated hearts were retrogradely perfused with a 5% CO_2-95% O_2-saturated modified Krebs–Henseleit (118.5 mM NaCl, 25 mM $NaHCO_3$, 4.7 mM KCl, 1.2 mM $MgSO_4$, 1.2 mM KH_2PO_4) buffer (1.4 mM Ca^{++}; 11 mM glucose) at a constant flow rate of 2.5 mL/min (Masterflex L/S peristaltic pump) at 37°C with an imposed pacing (9 Hz, 540 bpm). Hearts were stabilized for 20 min in these conditions then subjected to a normothermic, 30 min global ischemia by switching off the coronary perfusion. Hearts were then re-perfused for 30 min. Heart linear contractions were measured by passing a hook through the heart apex with a pre-load of 1.5 g and recorded. Perfusion pressure was recorded with a Labtrax 4/24T (World Precision Instruments) device and integrated using the LabScribe data acquisition and analysis software (v 2.0). Ex vivo preconditioning was achieved by submitting hearts to an iterative (4 times) ischemia-reperfusion sequence (2x 5 min)(see Fig. 1a).

Infarct sizes were measured using the 2,3,5-triphenyltetrazolium chloride (TTC) staining method. TTC (1%) was injected through the aortic canulae and incubated for 10 min at 37°C. Infarcted (white) and viable (red) areas were measured by computerized planimetry (Adobe Photoshop). Exclusion criteria for perfused hearts were a time to perfusion >3 min, a coronary perfusion pressure > 140 mm Hg or < 40 mm Hg or raising transiently above 180 mm Hg.

Cell lines and human primary ventricular cardiomyocytes

The AC16 human cardiomyocyte cell line [21] was from Millipore (SCC109). Cells were maintained in DMEM/F12 Ham (Sigma-Aldrich) supplemented with 2mM L-glutamine (Thermo Fisher Scientific), 12.5% of fetal bovine serum (FBS) and 1% penicillin-streptomycin (Thermo Fisher Scientific).

The U2OS cell line was from ATCC (HTB-96) and maintained in McCoy 5A medium (Thermo Fisher Scientific) supplemented with 10% FBS and 1% penicillin–streptomycin.

Authenticated (STR-profiled) HepG2 cells were from ATCC (HB-8095) and grown in DMEM containing 25 mM Glc supplemented with 10% FBS, 1 mM nonessential amino acids, 1 mM sodium pyruvate, and 1% penicillin/streptomycin.

Human primary ventricular cardiomyocytes were from PromoCell (C-12811). These cells are from ventricles of an explanted heart of a male donor who underwent heart transplantation. Cells were tested and validated for cell specific markers, morphology, viability and adherence rate. Cells were maintained in Myocyte Growth Medium (C-22070, PromoCell) supplemented with Myocyte growth medium supplement mix (C-39270, PromoCell).

For all experiments, confluent cells were synchronized using 100nM dexamethasone (Sigma) for 2 hours, then washed in 1x PBS. This defined T_0, after which cells were maintained in their respective growth media for further experimentation. Cell sampling and treatment were performed at indicated times. Cell viability was determined at indicated concentrations (see Fig. legends) using CellTiter-Glo® Luminescent Cell Viability Assay (Promega, G7570). DMSO was used at concentrations below 0.02% to avoid unwanted effects on REV-ERBα protein stability. Luciferase real-time recording was as described [33], with a stabilization period (T_0-T_{12}).

All cell lines were routinely (once a month) monitored for mycoplasma.

RNA extraction and RT-qPCR analysis

RNA extraction from cultured cells was carried out using the NucleoSpin® RNA Midi kit (Macherey-Nagel). Total RNA from mouse heart was extracted from samples pulverized in liquid nitrogen using TRIzol™ Reagent (Thermo Fisher Scientific). Prior to cDNA preparation with the High Capacity cDNA Reverse Transcription kit (Thermo Fisher Scientific), total RNA extracts were subjected to DNase I treatment. cDNAs were quantified using TaqMan Gene Expression Assays. Gene expression was normalized to 18S rRNA expression and relative gene expressions were calculated using the $2^{-\Delta\Delta Ct}$ method [70].

Protein extraction, Western blotting (WB) and Simple Western immunoassays

Proteins were extracted using M-PER cell lysis buffer (Pierce) supplemented with Halt Protein Phosphatase and Protease cocktail (1:100 dilution, Pierce). Following a brief vortexing and centrifugation (30 min., 16,000 G), the supernatant protein concentration was determined using the BCA protein assay kit (Pierce).

Protein expression level was studied either by western blotting or by WES Simple Western analysis (Simple Western™) [71].

- Western blotting: 20µg of protein were resolved by 12% SDS-PAGE under reducing conditions and blotted onto a nitrocellulose membrane. The membrane was blocked in 5% BSA in 1x TRIS-buffered Saline-Tween (TBS-T) and incubated overnight with the indicated antibody. Membranes were washed 3 times in 1x TBS-T and incubated with an anti-mouse HRP-labelled secondary antibody (1:10,000) for 1 hour. SuperSignal™ West Dura Extended Duration substrate (Thermo Fisher Scientific) was used to detect antigen-antibody complexes.
- WES analysis: 3.8 µg proteins were resolved by size by capillary electrophoresis. After immobilization onto the capillary by photoactivated capture chemistry, target proteins were identified using specific primary antibodies (see Supplemental Information for references) and immunoprobed using an HRP-conjugated secondary antibody and a chemiluminescent substrate (ProteinSimple). Chemiluminescent signals were detected and quantified using the Compass for SW software (ProteinSimple).

Protein levels were normalized to relative changes in HSP90AA1, β-actin or vinculin as indicated, which were run in parallel on different gels/WES plates at the same time using the same biological samples.

Cloning and transfection

Transfections were performed 24 hours (T_{-24}) prior to dexamethasone-induced synchronization. The pEZ-M11-hREV-ERBα (plasmid Genecopoeia) (referred to as Flag-REV-ERBα) was used to overexpress flagged human REV-ERBα or its derivatives. Human flagged REV-ERBα mutant (hREV-ERBα-H602F) deficient in binding heme was generated using the Flag-REV-ERBα plasmid by substituting H602 with F [72].

The human *Bmal1*-luciferase construct (Bmal-Luc) used for real-time bioluminescence studies was obtained by cloning the *Bmal1* promoter region (-350 to + 100) relative to the gene transcriptional start site into the SV40-driven, red-emitting luciferase pCBR reporter vector (Promega). Overexpression of wild type and constitutively active HIF1α was achieved by using HA-HIF1α-pcDNA3 (WT-HIF1α) and HA-HIF1α P402A/P564A-pcDNA3 (CA-HIF1α), respectively [73]. These plasmids were provided by W. Kaelin (Addgene plasmid # 18949, RRID: Addgene #18955Fugene HD® (Promega) was used to transfect AC16 cells. Transfection of U2OS was achieved using JetPEI ® (Polyplus Transfection).

For immunoprecipitation experiments, 10µg pEZ-M11-REV-ERBα were transfected into $1.1x10^7$ AC16 or U2OS cells. Transfection efficiency was controlled by RT-qPCR, western blotting or WES analysis.

Small interfering RNA

Transfections were performed 24 hours (T_{-24}) prior to dexamethasone-induced synchronization. AC16 cells were transfected for 24 hours with 10nM siRNAs (Control: On-target plus non-targeting pool or On-target plus Smart pool siRNAs; see details in the Appendix) using Lipofectamine RNAiMAX (Thermo Fisher Scientific). Silencing experiments in U2OS cells were carried out by transfecting 10nM siRNAs using INTERFERin® (Polyplus Transfection). Silencing efficiency was monitored by RT-qPCR or western blotting.

Immunoprecipitation and ubiquitination assay

Using the Crosslink Magnetic IP/Co-IP kit (Pierce), immunoprecipitation was carried out as described earlier [33]. For ubiquitination assays, $1.7x10^7$ cells were transfected with 10µg pEZ-M11-REV-ERBα plasmid. On the following day, cells were treated with 0.5µM digoxin (Sigma-Aldrich) with or without 1 µM clasto-lactacystin β-lactone (Sigma-Aldrich) or 10µM bortezomib (Sigma-Aldrich) for 24 hours. Ubiquitinylated proteins were captured using, the UBI-CAPTURE-Q® kit (ENZO Life Sciences). Ubiquitinylated proteins were resolved by 10% SDS-PAGE and were probed with anti-REV-ERBα antibody (Cell Signaling Tech.) or the anti-mono/polyubiquitinylated conjugates monoclonal antibody FK2 (ENZO Life Sciences).

PamGene Kinase Array

- **Sample preparation:** AC16 cells were plated in 12-well fibronectin-gelatin coated plates (Sigma). Cells were synchronized using 100nM dexamethasone as described above. Twenty hours later, cells were treated with 0.5 or 5µM digoxin. After 4 hours of incubation, cells were washed twice with 250 µL 1x PBS and lysed in 250 µL M-PER cell lysis buffer (Pierce) supplemented with Halt Protein Phosphatase and protease inhibitors (Pierce). Lysates were vortexed for 30 seconds and centrifugated (30 min., 16,000 G, 4°C). Protein concentration was determined with the BCA protein assay kit (Pierce).
- **PamStation Kinomic analysis:** Kinomic profiling of lysates was performed using a PamStation®12 (PamGene Intl) and Serine/Threonine Kinase (STK) PamChip® Arrays. Each STK PamChip® Array contains 144 peptides: 4 positive control phosphorylated peptides and 140 consensus phospho-peptide sequences representing the Ser/Thr kinome. Briefly, PamChip arrays were blocked with 2% BSA (1-30 cycles). After the initial blocking step, 2 µg proteins from cell lysates premixed with 4µl of 10x PK buffer (PamGene), 0.4 µl of 4mM ATP, 0.4 µl of

100x BSA, and 0.5 µl anti-STK primary antibody adjusted to a total volume of 40 µl in distilled water were added to individual PamChip arrays. The mix was then pumped (30 cycles) through the PamChip® then arrays were washed with 1x PBS/0.01% Tween buffer followed by injection of 30 µl of PamChip detection mix [0.4 µl of FITC-labelled anti-STK antibody (1 µg/µl in TRIS buffer, PamgGene), 3µl of 10x Ab buffer (PamGene) and 26.6 µl H_2O] . Real-time fluorescence signal was quantified by EVOLVE (PamGene.

- **Image and data analysis of kinomic profiles:** The BIONAVIGATOR software Suite (PamGene) was used to analyze images and to (log_2) transform signal intensities. The kinase upstream analysis algorithm within the BIONAVIGATOR Software Suite was employed to identify putatively active kinases. A final score is calculated by the software based on the scores obtained for specificity and significance. Kinases are ranked based on the mean final score (MFS). A heat map was plotted using MFS scores. To visualize kinase activity changes in digoxin-treated versus untreated cells/tissue, kinase trees were generated using the KinHub platform (http://www.kinhub.org/kinmap/).

Microarray analysis, term enrichment analysis and network analysis

Gene expression from mouse hearts or AC16 cells was analyzed with Affymetrix GeneChip Hu (or Mo)Gene 2.0 ST arrays after RNA amplification, sscDNA labeling and purification. RNA was amplified using the GeneChip™ WT PLUS Reagent Kit (Thermo Fisher Scientific), retrotranscribed to sscDNA and labeled using GeneChip™ WT Terminal Labeling Kit (Thermo Fisher Scientific), followed by hybridization on the GeneChip Mouse or Human Gene 2.0 ST Array (Affymetrix). Raw data were processed using GIANT (Galaxy-based interactive tools for Analysis of Transcriptomic data [74]. Using the GSEA module, normalized data were converted toward a GSEA compatible format for further analysis.

Real-time measurement of bioluminescence

Real-time monitoring of bioluminescence was performed using a Kronos AB-2550 luminometer (ATTO). AC16 or U2OS cells ($1.1x10^7$) were plated on P150 cell culture plates. When reaching 80% confluency, cells were transfected with the *Bmal*-Luc plasmid (10µg) using either Fugene HD® (Promega) or JetPEI® (Polyplus Transfection) for AC16 or U2OS cells, respectively. Twenty-four hours after transfection, cells were split into 35mm cell culture dishes. Cells were synchronized (100nM dexamethasone,2 hours) and the medium was replaced with AC16 or U2OS phenol red-free growth media. Cells were treated as indicated (see Fig. legends). Prior to starting light emission monitoring, 200 µM beetle luciferin (Promega) was added to growth medium. Bioluminescence was

609 measured for 1 min. at intervals of 10 min. under 5% CO_2 at 37°C for 4 days. Signals were quantified,
610 analyzed and detrended using the ATTO KRONOS software.
611
612 ***Rapid immunoprecipitation and mass spectrometry of endogenous proteins (RIME)***

613 RIME assays were performed using U2OS overexpressing Flagged-hREV-ERBα or HepG2 cells.
614 To overexpress REV-ERBα, cells were transfected with the Flag-REV-ERBα expression vector using
615 JetPEI (Polyplus transfection). Twenty-four hours after transfection, the medium was replaced by fresh
616 medium and cells were further incubated for 24h. Cells were synchronized (2h, 100 nM
617 dexamethasone), washed with 1x PBS and incubated for 20h with fresh media. Cells were cross-linked
618 for 10 min with 1% formaldehyde at 37°C in 1x DMEM. After quenching with 1.25 M glycine, cells were
619 washed twice with ice-cold 1x PBS. Fixed cells were scraped in ice-cold 1x PBS supplemented with
620 protease and phosphatase inhibitors (PIC, Roche). After centrifugation (1,000g, 10 min, 4°C), cells were
621 lysed in 50 mM HEPES-KOH pH 7.5, 140 mM NaCl, 1 mM EDTA, 10% glycerol, 0.5% NP40, 0.25% Triton
622 X-100 buffer supplemented with PIC. After centrifugation (1,000g, 10 min, 4°C), supernatants
623 (cytosolic fraction) and pellets (nuclear fraction) were collected. Pellets were washed in 10 mM TRIS-
624 HCl pH8.0, 200 mM NaCl, 1 mM EDTA and 0.5 mM EGTA buffer containing PIC , then in 10 mM TRIS-
625 HCl pH8.0, 200 mM NaCl, 1 mM EDTA and 0.5 mM EGTA, 0.1% sodium deoxycholate and 0.5% N-
626 laurylsarcosine buffer (with PIC). Nuclei were suspended into 50 mM HEPES-KOH pH 7.5, 1 mM EDTA,
627 0.5 M $LiCl_2$, 0.7% sodium deoxycholate, 1% NP40 and 1x PIC. After a 10 min sonication, Triton X-100
628 (1% v:v final) was added and samples were centrifuged at 20,000g for 10 min, yielding the nuclear
629 extract. In parallel, SureBeads™ Protein A or G magnetic beads (Bio-Rad) were saturated with 5 mg/mL
630 BSA. Four µg of rabbit monoclonal anti-REV-ERBα antibody (#13418, Cell Signalling Technology), 10 µg
631 of mouse monoclonal anti-Flag antibody (#F1804, Sigma-Aldrich), 10 µg of control rabbit IgG (sc-2027,
632 Santa Cruz Biotechnology) or mouse IgG (sc-2025, Santa Cruz Biotechnology) were immobilized on
633 SureBeads™ Protein A (Rabbit) or G (Mouse) magnetic beads.

634 After centrifugation, cytosolic or nuclear extracts were incubated overnight with immobilized
635 antibodies at 4°C. Beads were washed with 1x RIPA buffer [50 mM HEPES-KOH, pH 7.6, 1 mM EDTA,
636 0.7% (v:v) sodium deoxycholate, 1% (v:v) NP-40 and 0.5 M LiCl] then with 0.1 M ammonium hydrogen
637 carbonate. Beads were dried and flash-frozen in liquid nitrogen.LC-MS/MS analysis was performed to
638 identify REV-ERBα interactants as described [72].

639

640 ***Apoptosis and autophagy antibody arrays***

To evaluate global changes in the apoptosis and autophagic pathways in digoxin-treated cells, the Human Apoptosis Array C1 (AAH-APO-1-2, Raybiotech) and the Autophagy Array C1 (AAH-ATG-1-2, Raybiotech) were employed. These arrays detect 43 and 20 human proteins regulating apoptosis and autophagy, respectively. Briefly, AC16 cells were plated in P150 cell culture plates. At confluence, cells were synchronized as above. Eighteen hours post synchronization, cells were treated either with 0.5µM digoxin or vehicle and lysed 6h later (T_{24}) in lysis buffer (Raybiotech). Antibody arrays were blocked using the blocking buffer (2 mL, Raybiotech) for 30 minutes and 250µg of fresh total protein lysate (1 mL) was added to each antibody array (1 sample/array). Arrays were incubated overnight at 4°C, then washed thoroughly in washing buffer (1 mL/wash, Raybiotech) and were further incubated overnight at 4°C with biotinylated antibody cocktail (1 mL, Raybiotech). Arrays were washed twice (1 mL/wash) then incubated in 1x HRP-Streptavidin Concentrate for 2h at room temperature. All blocking, washing and incubation steps were performed under gentle rotation (0.5-1 cycle/sec). After a 2h incubation, arrays were washed once followed by chemiluminescence detection using an Invitrogen™ iBright™ FL1500 Imaging System (Thermo Fisher Scientific). Spot intensities on each array were quantified using Image Studio™ Lite (LI-COR Biosciences). The RayBiotech Microsoft® Excel-based analysis software tool was used to average, normalize and subtract the background signal. Heatmaps were generated using GraphPad Prism (v. 9.4).

Statistics and reproducibility

Statistical analysis was performed using GraphPad Prism (v. 9.4). Data are plotted as the mean ± SEM. At least 3 independent experimental replicates were obtained. In vitro data were determined to have equal variances using the F test. For 2-group comparisons, an unpaired 2-tailed *t*-test with Welch correction was used. For multiple comparisons with one variable, a 1-way ANOVA followed by the Tukey multiple comparison test (each group compared to every other group) was used. Multiple comparisons with more than one variable were carried out using a 2-way ANOVA followed by a Tukey's multiple comparison test. Cyclical patterns of gene expression or of protein levels were determined using JTK_Cycle [75]. Individual expression/level data were plotted in Prism as a time series and non-linearly fitted using the "sine wave with nonzero baseline" function, using a wavelength constraint previously determined by JTK_cycle (in the 20-24 hours range). For infarct size measurements, based on an observed standard deviation of 8%, with α set at 0.05, β at 0.20 and a size effect of 10%, the group size was set at n=7. In vivo datasets were considered to have unequal variances and groups were compared using either a one-sided Welch's t-test, or a Welch ANOVA followed by the Dunnett multiple comparison test unless mentioned otherwise. In all instances, P values < 0.05 were considered statistically significant. All samples used in this study were biological replicates, not

technical replicates. All experiments were independently performed at least twice to reproduce similar results.

Differential gene expression was analyzed after normalization of signals to the median of all samples, $\log_2$ transformation and exclusion of the 10^{th} lowest percentile considered as technically unreliable. The Limma package, based on an Empirical Bayes method, is embedded into the Giant suite and was used to identify genes exhibiting an expression fold-change > 1.2 with an FDR < 0.05 (moderated t-test followed by a Benjamini-Hochberg multiple testing correction). Biological term enrichment analysis was performed using the DAVID NCBI portal (v6.8) [76].

Reporting summary

Further information on research design is available in the Nature Research Reporting Summary linked to this article.

Data availability

All data are available in the main text or the supplementary materials. Source data are available for this paper. Microarray data that support the finding of this study has been deposited in the National Center of Biotechnology Information's Gene Expression Omnibus and are accessible through accession number GSE183659, GSE183660 and GSE183661. Other transcriptomic datasets have been described in [10] and deposited under the accession number GSE62459. Whole mouse heart circadian gene expression was analyzed using the GSE180108 dataset [47]. The mass spectrometry proteomics data have been deposited to the ProteomeXchange Consortium via the PRIDE [77] partner repository with the dataset identifier PXD03660

ACKNOWLEDGMENTS

We are grateful to Dr J. Vandel for help with transcriptomic data visualization, Prof S. Susen (CHRU Lille, France) for generously providing DigiFab, and to Faris Naji (PamGene, Netherlands) for help and advices for the PamGene data analysis. This work was supported by grants from INSERM (PL), Région Hauts-de-France and Université de Lille (REV-ERBalpha/SAS20215, PL), from ANR [LABX EGID (ANR-10-LABX-0046, BS); ANR VasCal (ANR46-CE14-0001-01, BS), ANR-CE14-0003-01 (DM), ANR-18-CE17-0003-02 (DM); PreciDiab ANR-18-IBHU-0001; 20001891/NP0025517; 2019_ESR_11 (DM), ANR-17-CE14-0034 (JSA), from the Leducq Foundation (LEAN network 16CVD01, BS), from Institut Pasteur de Lille (CTRL Melodie, JSA), from the Fondation pour la Recherche Médicale (EQU202103012732, JSA). BS is a recipient of an Advanced ERC Grant (694717)

AUTHOR'S CONTRIBUTIONS STATEMENT

Conceptualization: MV, PL, BS; Methodology: MV, JSA, AB, AH, SC, JE, PL; Validation: MV, CG, AH, SC, AB, PL; Formal analysis: MV, PL; Investigation: MV, CG, XM, AB, AH, SC, RB; Resources: PL, BS, JE, HD, SD, DM, JSA; Data visualization: MV, PL; Supervision: PL, BS; Funding acquisition: PL, BS.

COMPETING INTERESTS STATEMENT

Nothing to report

FIGURE LEGENDS

Fig. 1. Time of the day- and REV-ERBα-dependent effects of digoxin in mouse heart. (a) Time of the day dependency of mouse heart sensitivity to MIRI and preconditioning (PC). Upper panel: experimental outline. Lower panel: infarct sizes at ZT0 and ZT12, with or without prior exposure to an iterative short ischemia/reperfusion sequence. Results are shown as mean+/-SEM (n=8-9) which were compared using a two-way ANOVA test, followed by a Benjamini-Hochberg multiple comparison test. Infarct sizes were calculated based on necrosis area/area at risk. **(b)** Left panel: overrepresented Gene Ontology Biological Processes (GO BP) terms in differentially expressed genes (ZT0 vs ZT12) mouse hearts; right panel: up- or downregulated and/or rhythmically-expressed (period=22-24h) genes. **(c)** Time-dependent expression of mouse heart genes. Normalized expression data are expressed as mean +/-SEM (n=3). **(d)** MIRI at ZT0 or ZT9 in wild type mouse hearts after injection of vehicle or digoxin (IP: 1mg/kg). **Top:** experimental outline and representative transversal sections of TTC-stained mouse hearts post IR (red stain: healthy tissue, unstained: necrotic tissue); **Bottom**: infarct size measurements. Results are shown as mean+/-SEM (n=7-13) which were compared using two-way ANOVA test, followed by a Benjamini-Hochberg multiple comparison test. **(e)** REV-ERBα protein level in mouse heart whole extracts. Upper panel: representative Wes analysis of REV-ERBα protein levels in mouse whole hearts. Bottom panel: quantification of REV-ERBα protein levels as a function of time. Results are shown as mean+/-SEM (n=3-4, see also Supplementary Fig. 2a) which were and compared using Brown-Forsythe & Welch ANOVA test, followed by Dunnett's multiple comparison test. **(f)** In vivo digoxin ED_{50}. REV-ERBα levels were assessed at ZT9 in whole heart extracts. Results are shown as mean+/-SEM (n=9-16, see also Supplementary Fig. 2b) which were analyzed using nonlinear fit regression (least square method). **(g)** MIRI at ZT9. Myocardial IR tolerance was evaluated at ZT9 in wild type vs *Nr1d1*$^{-/-}$ or *Cdkn1a*$^{-/-}$ mouse hearts treated either with vehicle or digoxin (ZT5, IP: 1mg/kg). Results are shown as mean+/-SEM (n=6-7) which were compared using a two-tailed Welch's t-test. All measurements were from distinct samples.

Fig. 2. Digoxin affects REV-ERBα protein stability in a cell-autonomous manner. (a) Cyclic REV-ERBα protein levels in AC16 cells. Top panel: experimental outline. REV-ERBα levels were determined in synchronized human AC16 cells treated with vehicle or digoxin (0.5µM) at T_0 and harvested at T_0, T_6, T_{12}, T_{18} and T_{24}. Dex: dexamethasone. Bottom panel: Representative image from WES analysis. HSP90α was used as a protein loading control. Numbers indicate mean fold-changes [relative to maximal REV-ERBα expression (24h, untreated cells)]. Results are shown as mean+/-SEM (n=3) which were compared using a one-way ANOVA test, followed by a Tukey's multiple comparison test (see Extended data Fig. 3a). *: **: P<0.01, ***: P<0.005. **(b)** *NR1D1* and *BMAL1* mRNA expression in synchronized AC16 cells. Cells were treated with vehicle or digoxin (0.5µM) at T_0 and harvested at T_{24}

(n=5). Results are shown as mean+/-SEM (n=5) which were compared using an unpaired two-sided t-test. **(c)** Real-time monitoring of the *BMAL1* promoter activity. Top panel: experimental outline. Bottom panel: bioluminescence signal measured using a KRONOS (Atto) luminometer in AC16 cells transfected with the *Bmal1*-Luc(iferase) plasmid and treated with vehicle or digoxin (0.5 μM) (n=3). **(d)** CDKN1A/P21 protein level in AC16 cells. P21 level was assessed using the ProteinSimple Wes system in AC16 cells treated with vehicle or digoxin (0.5 μM). Results are shown as mean+/-SEM (n=5) which were compared using a unpaired two-sided t-test. ***: P<0.005. HSP90α was used as a protein loading control. All measurements were from distinct samples.

Fig. 3. Digoxin effect in human primary cardiomyocytes. (a) Rhythmic REV-ERBα protein level. Synchronized primary human cardiomyocyte cells were treated with vehicle or digoxin (0.5 μM) and harvested over a 36-hour period as indicated. (**b**) *NR1D1* and *BMAL1* mRNA expression in human primary cardiomyocytes. Normalized data are plotted as mean+/-SEM (n=5) and compared using a one-way ANOVA test, followed by a Tukey's multiple comparison test. Vinculin was used as a protein loading control. All measurements were from distinct samples.

Fig. 4. Intracellular pathways activation by digoxin. (a) NKA ion pumping vs signalosome activities. Top panel: experimental outline. Synchronized AC16 cells were treated as indicated for 6 hours at T18 and harvested at T_{24}. Dex: dexamethasone. Bottom panel: REV-ERBα protein levels in control and treated cells. HSP90α was used as a protein loading control. Right panel: normalized REV-ERBα protein level. Results are shown as mean+/-SEM (n=10, see also Supplementary Fig. 7) which were compared using a one-way ANOVA test, followed by a Tukey's multiple comparison test. **(b,c)** Kinase activation trees in AC16 cells generated by KinMap using kinase profiling data at low **(b)** or high **(c)** digoxin treatment concentration. Circle diameters are proportional to the level of activity of kinases. **(d)** Heat map quantifying dose-dependent changes in kinase activities (n=3; 1-way ANOVA, *: P<0.05). MFS: median final score. **(e)** Transcriptomic analysis in vehicle- or digoxin-treated (0.5μM, 5μM) AC16 cells. The heatmap shows the top-ranking 25 genes and indicates dose-dependent changes in mRNA expression. Stars indicate genes whose expression is also altered in mouse heart after digoxin treatment at ZT9. **(f)** Gene set enrichment analysis of upregulated genes in digoxin-treated AC16 cells.

Fig. 5. Target screening with kinase specific and pathway specific inhibitors. REV-ERBα protein levels were quantified after a 6 hour-treatment (at T_{18}) with or without digoxin and with or without enzyme inhibitors: **(a)** PP2 (20μM, Src kinase inhibitor), **(b)** ZSTK474 (10μM, PI3 kinase inhibitor), **(c)** SCH772984 (20μM, ERK 1&2 inhibitor), **(d)** MK2206 (1μM, AKT1/2/3 kinase inhibitor), **(e)** KN93 (1μM, CAMK 2&4 inhibitor), **(f)** PD98059 (20μM, MEK 1&2 inhibitor), **(g)** RP-8-pCPT-cGMPS (20μM, PKG1&2), **(h)** CRT0066101 (5μM, PKD inhibitor), **(i)** PF-4708671 (10μM, P70S6K1 inhibitor), **(j)** BAY11-7082 (10μM,

LUBAC and UPS inhibitor), **(k)** HOIPIN8 (10µM, LUBAC-HOIP specific inhibitor), **(l)** BMS-345541 (10µM, IKK α/β inhibitor), **(m)** TPCA-1 (20nM, IKKβ **(n)** Amlexanox (20µM, IKKε & TBK1 inhibitor). HSP90α was used as a protein loading control. Results are shown as mean+/-SEM (n=3-6) which were compared using a one-way ANOVA test, followed by a Tukey's multiple comparison test. All measurements were from distinct samples.

Fig. 6. Digoxin triggers REV-ERBα protein degradation through UPS. REV-ERBα protein levels were quantified after a 6 hour-treatment with or without digoxin and with or without the following proteasome inhibitors in synchronized AC16 cells **(a)** clasto-lactacystin β-lactone (10µM, proteasomal inhibitor), **(b)** bortezomib (BTZ, 200nM, PSMB5 inhibitor) and in synchronized U2OS cells **(c)** treated with either vehicle, digoxin (0.5µM) and/or bortezomib (200nM, PSMB5 inhibitor. Results are shown as mean+/-SEM (n=3-6) which were compared using a one-way ANOVA test, followed by a Tukey's multiple comparison test. **(d)** Normalized REV-ERBα protein level was assessed in synchronized AC16 cells transfected with Flag-Rev-ERBα or Flag-Rev-ERBα-H602F-encoding plasmids and treated with vehicle or digoxin (0.5µM). HSP90α was used as a protein loading control Results are shown as mean+/-SEM (n=5) which were compared using a one-way ANOVA test, followed by a Tukey's multiple comparison test. **(e)** Western blot analysis of total ubiquitinylated proteins and of ubiquitinated REV-ERBα protein from cell lysates of U20S cells transfected with Flag-Rev-ERBα plasmid and treated with either vehicle, digoxin (0.5µM) and/or bortezomib (BTZ, 200nM, PSMB5 inhibitor) for 2 hours (T18 to T20). Mono- and poly-ubiquitinylated proteins in the lysate were enriched by passing it through a High binding affinity UBI-QAPTURE-Q® matrix. All measurements were from distinct samples. *: P<0.05, **: P<0.01, ***: P<0.001, ****: P<0.0001.

Fig. 7. UPS-related REV-ERBα interactants. (a) REV-ERBα interactants extracted from the RIME dataset filtered against the Gene Ontology "cellular component" or "molecular functions" databases using "proteasome" or "ubiquitin" as biological terms. Green lines indicate known direct interactions as extracted from the String database. Red lines indicate detected direct or indirect interactions with REV-ERBα by RIME. Distances between REV-ERBα and interactants are inversely proportional to the number of identified peptides in the RIME data. Protein structures are from the AlphaFold Protein Structure database. **(b)** Outcome of REV-ERBα interactant inhibition on digoxin-induced REV-ERBα degradation. The table indicates the list of targets (identified from RIME and literature survey) studied here using siRNA- and/or inhibitor-based strategies, and the outcome of such inhibition on REV-ERBα protein level levels. Upward arrow: increased REV-ERBα protein level; downward arrow: decreased REV-ERBα protein level; equal sign: no change.

Fig. 8: Hypothetical scheme for digoxin action in cardiomyocytes. The main pathways activated by digoxin and the impact thereof on REV-ERBα protein stability are shown. More details can be found in the text.

REFERENCES

1 Patke, A., Young, M. W. & Axelrod, S. Molecular mechanisms and physiological importance of circadian rhythms. *Nat Rev Mol Cell Biol* **21**, 67-84 (2020).

2 Martino, T. A. & Young, M. E. Influence of the cardiomyocyte circadian clock on cardiac physiology and pathophysiology. *J Biol Rhythms* **30**, 183-205 (2015).

3 Zhang, J., Chatham, J. C. & Young, M. E. Circadian Regulation of Cardiac Physiology: Rhythms That Keep the Heart Beating. *Annu Rev Physiol* **82**, 79-101 (2020).

4 Crnko, S., Du Pre, B. C., Sluijter, J. P. G. & Van Laake, L. W. Circadian rhythms and the molecular clock in cardiovascular biology and disease. *Nat Rev Cardiol* **16**, 437-447 (2019).

5 Hausenloy, D. J. & Yellon, D. M. Myocardial ischemia-reperfusion injury: a neglected therapeutic target. *J Clin Invest* **123**, 92-100 (2013).

6 Hausenloy, D. J. & Yellon, D. M. Ischaemic conditioning and reperfusion injury. *Nat Rev Cardiol* **13**, 193-209 (2016).

7 Rossello, X. & Yellon, D. M. The RISK pathway and beyond. *Basic Res Cardiol* **113**, 2 (2018).

8 Durgan, D. J. *et al.* Short communication: ischemia/reperfusion tolerance is time-of-day-dependent: mediation by the cardiomyocyte circadian clock. *Circ Res* **106**, 546-550 (2010).

9 Janszky, I. L., R. Shifts to and from Daylight Saving Time and Incidence of Myocardial Infarction. *N Engl J Med* **359**, 1966-1968 (2008).

10 Montaigne, D. *et al.* Daytime variation of perioperative myocardial injury in cardiac surgery and its prevention by Rev-Erbα antagonism: a single-centre propensity-matched cohort study and a randomised study. *The Lancet* **391**(10115),59-69. (2018).

11 Davidson, S. M. *et al.* Multitarget Strategies to Reduce Myocardial Ischemia/Reperfusion Injury: JACC Review Topic of the Week. *J Am Coll Cardiol* **73**, 89-99 (2019).

12 Fellahi, J. L., Fischer, M. O., Daccache, G., Gerard, J. L. & Hanouz, J. L. Positive Inotropic Agents in Myocardial Ischemia–Reperfusion Injury. *Anesthesiology* **118**, 1460-1472 (2013).

13 Matsui, H. & Schwartz, A. Mechanism of cardiac glycoside inhibition of the (Na+-K+)-dependent ATPase from cardiac tissue. *Biochim Biophys Acta* **151**, 655-663 (1968).

14 Askari, A. The sodium pump and digitalis drugs: Dogmas and fallacies. *Pharmacol Res Perspect* **19**,7:e00505 (2019).

15 Liang, M. *et al.* Identification of a pool of non-pumping Na/K-ATPase. *J Biol Chem* **282**, 10585-10593 (2007).

16 Marck, P. V. & Pierre, S. V. Na/K-ATPase Signaling and Cardiac Pre/Postconditioning with Cardiotonic Steroids. *Int J Mol Sci* **19**,2336 (2018).

17 Nelson, W., Kupferberg, H. & Halberg, F. Dose-response evaluations of a circadian rhythmic change in susceptibility of mice to ouabain. *Toxicol Appl Pharmacol* **18**, 335-339 (1971).

18 Patocka, J., Nepovimova, E., Wu, W. & Kuca, K. Digoxin: Pharmacology and toxicology-A review. *Environ Toxicol Pharmacol* **79**, 103400 (2020).

19 Dostanic, I. *et al.* The alpha2 isoform of Na,K-ATPase mediates ouabain-induced cardiac inotropy in mice. *J Biol Chem* **278**, 53026-53034 (2003).

20 Iisalo, E. Clinical pharmacokinetics of digoxin. *Clinical pharmacokinetics* **2**, 1-16 (1977).

21 Davidson, M. M. *et al.* Novel cell lines derived from adult human ventricular cardiomyocytes. *J Mol Cell Cardiol* **39**, 133-147 (2005).

22 Felippe Gonçalves-de-Albuquerque, C., Ribeiro Silva, A., Ignácio da Silva, C., Caire Castro-Faria-Neto, H. & Burth, P. Na/K Pump and Beyond: Na/K-ATPase as a Modulator of Apoptosis and Autophagy. *Molecules* **22**, 578 (2017).

23 Balsalobre, A., Marcacci, L. & Schibler, U. Multiple signaling pathways elicit circadian gene expression in cultured Rat-1 fibroblasts. *Curr Biol* **10**, 1291-1294 (2000).

24 Katz, A. *et al.* Selectivity of digitalis glycosides for isoforms of human Na,K-ATPase. *J Biol Chem* **285**, 19582-19592 (2010).

25 Morgan, E. E. *et al.* Preconditioning by subinotropic doses of ouabain in the Langendorff perfused rabbit heart. *Journal of cardiovascular pharmacology* **55**, 234-239 (2010).

26 Duan, Q. *et al.* Preconditioning and Postconditioning by Cardiac Glycosides in the Mouse Heart. *Journal of cardiovascular pharmacology* **71**, 95-103 (2018).

27 Zhang, Z. *et al.* Identification of hydroxyxanthones as Na/K-ATPase ligands. *Mol Pharmacol* **77**, 961-967 (2010).

28 Orlov, S. N. *et al.* Na(+)i,K(+)i-Dependent and -Independent Signaling Triggered by Cardiotonic Steroids: Facts and Artifacts. *Molecules* **22**, 635 (2017).

29 Huh, J. R. *et al.* Digoxin and its derivatives suppress TH17 cell differentiation by antagonizing RORgammat activity. *Nature* **472** (2011).

30 Ouyang, X. *et al.* Digoxin Suppresses Pyruvate Kinase M2-Promoted HIF-1alpha Transactivation in Steatohepatitis. *Cell Metab* **27**, 339-350 (2018).

31 Zhang, H. *et al.* Digoxin and other cardiac glycosides inhibit HIF-1alpha synthesis and block tumor growth. *Proc Natl Acad Sci U S A* **105**, 19579-19586 (2008).

32 Strickson, S. *et al.* The anti-inflammatory drug BAY 11-7082 suppresses the MyD88-dependent signalling network by targeting the ubiquitin system. *Biochem J* **451**, 427-437 (2013).

33 Oikawa, D. *et al.* Molecular bases for HOIPINs-mediated inhibition of LUBAC and innate immune responses. *Commun Biol* **3**, 163 (2020).

34 Xie, Z. *et al.* Gene Set Knowledge Discovery with Enrichr. *Current protocols* **1**, e90 (2021).

35 Brown, K., Gerstberger, S., Carlson, L., Franzoso, G. & Siebenlist, U. Control of I kappa B-alpha proteolysis by site-specific, signal-induced phosphorylation. *Science* **267**, 1485-1488 (1995).

36 Wang, Y. *et al.* Cardiac glycosides induce autophagy in human non-small cell lung cancer cells through regulation of dual signaling pathways. *Int J Biochem Cell Biol* **44**, 1813-1824 (2012).

37 Raghuram, S. *et al.* Identification of heme as the ligand for the orphan nuclear receptors REV-ERBalpha and REV-ERBbeta. *Nat Struct Mol Biol* **14**, 1207-1213 (2007).

38 Carter, E. L., Gupta, N. & Ragsdale, S. W. High Affinity Heme Binding to a Heme Regulatory Motif on the Nuclear Receptor Rev-erbbeta Leads to Its Degradation and Indirectly Regulates Its Interaction with Nuclear Receptor Corepressor. *J Biol Chem* **291**, 2196-2222 (2016).

39 Mohammed, H. *et al.* Rapid immunoprecipitation mass spectrometry of endogenous proteins (RIME) for analysis of chromatin complexes. *Nat Protoc* **11**, 316-326 (2016).

40 DeBruyne, J. P., Baggs, J. E., Sato, T. K. & Hogenesch, J. B. Ubiquitin ligase Siah2 regulates RevErbalpha degradation and the mammalian circadian clock. *Proc Natl Acad Sci U S A* **112**, 12420-12425 (2015).

41 Zhao, X. *et al.* Circadian Amplitude Regulation via FBXW7-Targeted REV-ERBalpha Degradation. *Cell* **165**, 1644-1657 (2016).

42 Yin, L., Joshi, S., Wu, N., Tong, X. & Lazar, M. A. E3 ligases Arf-bp1 and Pam mediate lithium-stimulated degradation of the circadian heme receptor Rev-erb alpha. *Proc. Natl. Acad. Sci. U. S. A* **107**, 11614-11619 (2010).

43 Li, Y. *et al.* An integrated bioinformatics platform for investigating the human E3 ubiquitin ligase-substrate interaction network. *Nat Commun* **8**, 347 (2017).

44 Yin, L., Wang, J., Klein, P. S. & Lazar, M. A. Nuclear receptor Rev-erba is a critical lithium-sensitive component of the circadian clock. *Science* **311**, 1002-1005 (2006).

45 Hill, R. J. W., Innominato, P. F., Levi, F. & Ballesta, A. Optimizing circadian drug infusion schedules towards personalized cancer chronotherapy. *PLoS Comput Biol* **16**, e1007218 (2020).

46 Hermida, R. C. *et al.* Bedtime hypertension treatment improves cardiovascular risk reduction: the Hygia Chronotherapy Trial. *Eur Heart J* **41**, 4565-4576 (2020).

47 Martino, T. *et al.* Day/night rhythms in gene expression of the normal murine heart. *J Mol Med (Berl)* **82**, 256-264 (2004).

48 Podobed, P. *et al.* The day/night proteome in the murine heart. *Am J Physiol Regul Integr Comp Physiol* **307**, R121-137 (2014).

49 Duan, Q. *et al.* Role of phosphoinositide 3-kinase IA (PI3K-IA) activation in cardioprotection induced by ouabain preconditioning. *J Mol Cell Cardiol* **80**, 114-125 (2015).

50 Digitalis Investigation, G. The effect of digoxin on mortality and morbidity in patients with heart failure. *N Engl J Med* **336**, 525-533 (1997).
51 Hallberg, P., Lindbäck, J., Lindahl, B., Stenestrand, U. & Melhus, H. Digoxin and mortality in atrial fibrillation: a prospective cohort study. *European journal of clinical pharmacology* **63**, 959-971 (2007).
52 Patel, N. J. *et al.* Digoxin significantly improves all-cause mortality in atrial fibrillation patients with severely reduced left ventricular systolic function. *Int J Cardiol* **169**, e84-86 (2013).
53 Rana, S., Prabhu, S. D. & Young, M. E. Chronobiological Influence Over Cardiovascular Function: The Good, the Bad, and the Ugly. *Circ Res* **126**, 258-279 (2020).
54 Young, M. E. *et al.* Cardiomyocyte-specific BMAL1 plays critical roles in metabolism, signaling, and maintenance of contractile function of the heart. *J Biol Rhythms* **29**, 257-276 (2014).
55 Tsimakouridze, E. V. *et al.* Chronomics of pressure overload-induced cardiac hypertrophy in mice reveals altered day/night gene expression and biomarkers of heart disease. *Chronobiol Int* **29**, 810-821 (2012).
56 Carter, E. L., Ramirez, Y. & Ragsdale, S. W. The Heme Regulatory Motif of Nuclear Receptor Rev-erbbeta is a Key Mediator of Heme and Redox Signaling in Circadian Rhythm Maintenance and Metabolism. *J Biol Chem* **292**, 11280-11299 (2017).
57 Wang, J. & Lazar, M. A. Bifunctional role of Rev-erbalpha in adipocyte differentiation. *Mol. Cell Biol* **28**, 2213-2220 (2008).
58 Kaasik, K. & Lee, C. C. Reciprocal regulation of haem biosynthesis and the circadian clock in mammals. *Nature* **430**, 467-471 (2004).
59 Dioum, E. M. *et al.* NPAS2: A Gas-Responsive Transcription Factor. *Science* **298**, 2385-2387 (2002).
60 Yang, J. *et al.* A novel heme-regulatory motif mediates heme-dependent degradation of the circadian factor period 2. *Mol Cell Biol* **28**, 4697-4711 (2008).
61 Reitz, C. J. *et al.* SR9009 administered for one day after myocardial ischemia-reperfusion prevents heart failure in mice by targeting the cardiac inflammasome. *Communications Biology* **2,** 353 (2019).
62 Mia, S. *et al.* Differential effects of REV-ERBalpha/beta agonism on cardiac gene expression, metabolism, and contractile function in a mouse model of circadian disruption. *Am J Physiol Heart Circ Physiol* **318**, H1487-H1508 (2020).
63 Zhang, L. *et al.* REV-ERBα ameliorates heart failure through transcription repression. *JCI Insight* **2**, e95177 (2017).

64 Stujanna, E. N. *et al.* Rev-erb agonist improves adverse cardiac remodeling and survival in myocardial infarction through an anti-inflammatory mechanism. *PLoS One* **12**, e0189330 (2017).

65 Zhao, Y. *et al.* Disruption of Circadian Rhythms by Shift Work Exacerbates Reperfusion Injury in Myocardial Infarction. *J Am Coll Cardiol* **79**, 2097-2115 (2022).

66 Busonero, C. *et al.* Ouabain and Digoxin Activate the Proteasome and the Degradation of the ERalpha in Cells Modeling Primary and Metastatic Breast Cancer. *Cancers (Basel)* **12**, 3840 (2020).

67 Wang, Y. *et al.* Bufalin is a potent small-molecule inhibitor of the steroid receptor coactivators SRC-3 and SRC-1. *Cancer Res* **74**, 1506-1517, doi:10.1158/0008-5472.Can-13-2939 (2014).

68 Woldt, E. *et al.* Rev-erb-alpha modulates skeletal muscle oxidative capacity by regulating mitochondrial biogenesis and autophagy. *Nat Med* **19**, 1039-1046 (2013).

69 Bell, R. M., Mocanu, M. M. & Yellon, D. M. Retrograde heart perfusion: the Langendorff technique of isolated heart perfusion. *J Mol Cell Cardiol* **50**, 940-950 (2011).

70 Schmittgen, T. D. & Livak, K. J. Analyzing real-time PCR data by the comparative CT method. *Nature Protocols* **3**, 1101-1108 (2008).

71 Harris, V. M. Protein detection by Simple Western™ analysis. *Methods Mol Biol* **1312**, 465-468 (2015).

72 Berthier, A. *et al.* Combinatorial regulation of hepatic cytoplasmic signaling and nuclear transcriptional events by the OGT/REV-ERBalpha complex. *Proc Natl Acad Sci U S A* **115**, E11033-E11042 (2018).

73 Kondo, K., Klco, J., Nakamura, E., Lechpammer, M. & Kaelin, W. G., Jr. Inhibition of HIF is necessary for tumor suppression by the von Hippel-Lindau protein. *Cancer Cell* **1**, 237-246 (2002).

74 Vandel, J. *et al.* GIANT: galaxy-based tool for interactive analysis of transcriptomic data. *Scientific Reports* **10**, 19835 (2020).

75 Hughes, M. E., Hogenesch, J. B. & Kornacker, K. JTK_CYCLE: an efficient nonparametric algorithm for detecting rhythmic components in genome-scale data sets. *J Biol Rhythms* **25**, 372-380 (2010).

76 Huang da, W., Sherman, B. T. & Lempicki, R. A. Systematic and integrative analysis of large gene lists using DAVID bioinformatics resources. *Nat Protoc* **4**, 44-57 (2009).

77 Perez-Riverol, Y. et al. The PRIDE database resources in 2022: a hub for mass spectrometry-based proteomics evidences. Nucleic Acids Res 50, D543-d552 (2022).

SUPPLEMENTAL DATA

Extended data Fig. 1. Rhythmic gene and protein level in mouse heart whole tissue extracts. **(a)** WES analysis of REV-ERBα protein level in mouse hearts collected over a 24-hours period at rest phase (ZT0-ZT12) and active phase (ZT13-ZT24) (n=4). HSP90α was used as a protein loading control. **(b)** WES analysis of REV-ERBα protein level in mouse hearts collected at ZT9 after vehicle or digoxin injection (0.1,0.5, and 0.1mpk at ZT5. **(c)** Cyclic *Nr1d1, Nr1d2, Bmal1 and Cdkn1a* mRNA expression in mouse hearts collected at rest (ZT0-ZT12) or active (ZT13-ZT24) phases Results are shown as mean+/-SEM (n=3). **(d)** *Nr1d1, Arntl (Bmal1) and Cdkn1a* mRNA expression in mouse hearts collected at ZT9 after vehicle or digoxin (1mpk) injection at ZT5. Results are shown as mean+/-SEM (n=8-9) which were compared using which were compared using a two-tailed Welch's t-test. **(e)** P21 protein level in mouse hearts collected at ZT9 after vehicle or digoxin (1mpk) injection at ZT5. **(f)** REV-ERBα protein level in mouse hearts collected at ZT0 after vehicle or digoxin (1mpk) injection at ZT20. Basal REV-ERBα protein level at ZT9 is shown here as reference. Measurements were from distinct samples. Quantification of data in panels (a), (b) and (c) appears in Fig. 1.

Extended data Fig. 2. NKA status in mouse heart and AC16 cells. (a) Left panel: NKA isotype-encoding mRNA expression in mouse heart. *Atp1a1*, *Atp1a2* and *Atp1a3* expression levels are plotted as a function of time. *Per1* mRNA expression is shown as a reference circadian gene. Middle panel: Relative expression of NKA isotype-encoding mRNA expression in mouse heart at ZT9. Results are shown as mean+/-SEM (n=8-15) which were compared using Brown-Forsythe & Welch ANOVA test, followed by Dunnett's multiple comparison test. Right panel: Effect of digoxin treatment on NKA isotype-encoding mRNA expression in mouse heart at ZT9. Results are shown as mean+/-SEM (n=8-15) which were compared using Brown-Forsythe & Welch ANOVA test, followed by Dunnett's multiple comparison test. **(b)** NKA isotype protein expression level in mouse heart as a function of time. Data quantification is shown (right panel) as mean+/-SEM (n=3) which were compared using a one-way ANOVA test, followed by a Tukey's multiple comparison test. *: P<0.05, **: P<0.01, ***: P<0.001**. (c)** Left panel: Relative expression of NKA isotype-encoding mRNA expression in human AC16 cells (T_{24}). Right panel: Effect of digoxin treatment on NKA isotype-encoding mRNA expression in human AC16 cells (T_{24}). Results are shown as mean+/-SEM (n=5-6) which were compared using a one-way ANOVA test, followed by a Tukey's multiple comparison test. **(d)** NKA isotype protein expression level in human AC16 as a function of time. Data quantification is shown (right panel) as mean+/-SEM (n=4) which were compared using a one-way ANOVA test, followed by a Tukey's multiple comparison test. All measurements were from distinct samples. *: P<0.05, **: P<0.01

Extended data Fig. 3. Effects of digoxin and of its structural analogs on REV-ERBα protein stability. **(a)** AC16 cellular viability in the presence of increasing concentrations of digoxin. Data are plotted as mean+/-SEM (n=4) which were compared using a one-way ANOVA test, followed by a Tukey's multiple comparison test. **(b)** Protein array analysis of AC16 whole cell protein extract. AC16 cells were treated for 6hours at T_{18} as indicated and extracts were probed on membrane spotted with antibodies specific for components of the apoptotic pathway. Fluorescence signals were quantified and were represented as a heatmap (n=2). **(c)** Cyclic REV-ERBα protein levels in human AC16 cells. REV-ERBα levels were determined in synchronized human AC16 cells treated with vehicle or digoxin (0.5μM) and harvested at T_0, T_6, T_{12}, T_{18} and T_{24}. Quantification of data is shown in Fig. 2A. **(d)** REV-ERBα protein level was assessed in AC16 cells treated with vehicle, digoxin (0.5 μM) and/or DigiFab (100μg). HSP90α was used as a protein loading control. Right panel: normalized data are plotted as mean+/-SEM (n=3) which were compared using a one-way ANOVA test, followed by a Tukey's multiple comparison test. **(e)** REV-ERBα protein level was assessed in AC16 cells treated with vehicle or varying concentration of digoxin as indicated. HSP90α was used as a protein loading control Right panel: normalized data are plotted as mean+/-SEM (n=3) and analyzed by nonlinear regression curve fitting. **(f)** REV-ERBα protein level in AC16 cells treated with vehicle or varying concentrations of bufalin (0.1, 1.0, 10μM) (n=2). **(g)** REV-ERBα protein level in AC16 cells treated with vehicle or ouabain (5μM) (n=2). HSP90α was used as a protein loading control. All measurements were from distinct samples. **(h)** Time course experiment in AC16 cells treated at T_{18} with vehicle or digoxin (5μM). REV-ERBα protein level was assessed using the ProteinSimple Wes system (n=2). HSP90α was used as a protein loading control. All measurements were from distinct samples. ***: P<0.001.

Extended data Fig. 4. Digoxin effect in U2OS cells. **(a)** Rhythmic REV-ERBα and RORα protein level in synchronized U2OS cells treated with vehicle or digoxin (0.5 μM) and harvested over a 36-hour period as indicated. HSP90α was used as a protein loading control. **(b)** *NR1D1* and *BMAL1* mRNA expression in synchronized U2OS cells treated with vehicle or digoxin (0.5 μM) and harvested at T_{24}. Normalized data are plotted as mean+/-SEM (n=6) which were compared using a one-way ANOVA test, followed by a Tukey's multiple comparison test. **(c)** Bioluminescent signal in U2OS cells transfected with the *Bmal1*-Luc plasmid and treated with vehicle or digoxin (0.5 μM). Detrended data are shown HSP90α was used as a protein loading control. All measurements were from distinct samples.

Extended data Fig. 5. Effect of protein kinase inhibition or activation on digoxin-mediated REV-ERBα protein level decrease. Representative WES analysis (related to quantified data in Fig. 4) are shown. REV-ERBα protein level in synchronized AC16 cells treated with REV-ERBα protein levels were quantified after a 6 hour-treatment with or without digoxin and with or without enzyme inhibitors: **(a)**

PP2 (20μM, Src kinase inhibitor), **(b)** ZSTK474 (10μM, PI3 kinase inhibitor), **(c)** SCH772984 (10μM, ERK 1&2 inhibitor), **(d)** MK2206 (1μM, AKT1/2/3 kinase inhibitor), **(e)** KN93 (10μM, CAMK 2&4 inhibitor), **(f)** PD98059 (10μM, MEK 1&2 inhibitor), **(g)** RP-8-pCPT-cGMPS (20μM, PKG1&2), **(h)** CRT0066101 (5μM, PKD inhibitor), **(i)** PF-4708671 (10μM, P70S6K1 inhibitor), **(j)** BAY11-7082 (10μM, LUBAC and UPS inhibitor), **(k)** HOIPIN8 (10μM, LUBAC-HOIP specific inhibitor), **(l)** TPCA-1 (20nM, IKKβinhibitor), **(m)** TPCA-1 (5μM, IKKβ/α inhibitor) **(n)** amlexanox (1μM, IKKε & TBK1 inhibitor). HSP90α was used as a protein loading control.

Extended data Fig. 6. Effect of protein kinase inhibition or activation on digoxin-mediated REV-ERBα protein level decrease. Quantification of REV-ERBα protein levels in synchronized human AC16 cells (see Extended data Fig. 7) **(a)** treated with vehicle, digoxin (0.5μM) and/or SRC inhibitor (saracatinib), (**b**) treated with vehicle, digoxin (0.5μM) and/or PI3K inhibitor (LY294002) **(c)** treated with vehicle, digoxin (0.5μM) and/or PI3K/P70S6K inhibitor (dactolisib), **(d)** transfected with ERK1 expression vector, **(e)** treated with the GSK3β inhibitor lithium and/or digoxin, **(f)** transfected with scrambled siRNA (Scr siRNA) or *CAMK4* siRNA and treated with vehicle or digoxin (0.5μM), **(g)** transfected with scrambled siRNA (Scr siRNA) or *ERK1&3* siRNA and treated with vehicle or digoxin (0.5μM), **(h)** transfected with scrambled siRNA (Scr siRNA) or *PKD1* siRNA and treated with vehicle or digoxin (0.5μM), **(i)** transfected with scrambled siRNA (Scr siRNA) or *PRKG1* siRNA and treated with vehicle or digoxin (0.5μM), **(j)** transfected with scrambled siRNA (Scr siRNA) or *HOIL* siRNA and treated with vehicle or digoxin (0.5μM) and **(k)** transfected with an empty (pcDNA3) or OTULIN-expressing (pcDNA3-*OTULIN*) vector and treated with vehicle or digoxin (0.5μM). Normalized data are plotted as mean+/-SEM (n=3-6) and compared using a one-way ANOVA test, followed by a Tukey's multiple comparison test except for **(c)** for which groups were compared using an unpaired 2-tailed *t*-test. All measurements were from distinct samples.

Extended data Fig. 7. Effect of protein kinase inhibition or activation on digoxin-mediated REV-ERBα protein level decrease. WES analysis of REV-ERBα protein levels in synchronized human AC16 cells **(a)** treated with vehicle, digoxin (0.5μM) and/or SRC inhibitor (saracatinib, 10μM), (**b**) treated with vehicle, digoxin (0.5μM) and/or PI3K inhibitor (LY294002, 20μM) **(c)** treated with vehicle, digoxin (0.5μM) and/or PI3K/P70S6K inhibitor (dactolisib, 0.1μM), **(d)** transfected with ERK1 expression vector, **(e)** treated with the GSK3β inhibitor lithium (20mM) and/or digoxin, **(f)** transfected with scrambled siRNA (Scr siRNA) or *CAMK4* siRNA and treated with vehicle or digoxin (0.5μM), **(g)** transfected with scrambled siRNA (Scr siRNA) or *ERK1&3* siRNA and treated with vehicle or digoxin (0.5μM), **(h)** transfected with scrambled siRNA (Scr siRNA) or *PKD1* siRNA and treated with vehicle or digoxin (0.5μM), **(i)** transfected with scrambled siRNA (Scr siRNA) or *PKG1* siRNA and treated with vehicle or digoxin (0.5μM), **(j)** transfected with scrambled siRNA (Scr siRNA) or *HOIL* siRNA and treated with

vehicle or digoxin (0.5µM) and **(k)** transfected with an empty (pcDNA3) or OTULIN-expressing (pcDNA3-*OTULIN*) vector and treated with vehicle or digoxin (0.5µM).

Extended data Fig. 8. Proteasome inhibition counteracts digoxin effect on REV-ERBα levels. Quantification of data appears in Fig. 5. REV-ERBα protein level in synchronized AC16 cells **(a)** treated with either vehicle, digoxin (0.5µM) and/or clasto-lactacystin β-lactone (10µM, proteasomal Inhibitor), **(b)** treated with either vehicle, digoxin (0.5µM) and/or bortezomib (200nM, PSMB5 inhibitor), in synchronized U2OS cells treated **(c)** with either vehicle, digoxin (0.5µM) and/or bortezomib (200nM, PSMB5 inhibitor)in synchronized AC16 cells **(d)** in synchronized AC16 cells transfected with Flag-Rev-ERBα or Flag-Rev-ERBα-H602F then treated with vehicle or digoxin (0.5µM). HSP90α was used as a protein loading control.

Extended data Fig. 9. Screening E2/E3 ligases potentially involved in digoxin-induced REV-ERBα degradation. (a) Quantification of REV-ERBα protein level in AC16 cells transfected either with scrambled siRNA (Scr siRNA) or *SIAH2* siRNA and treated with vehicle or digoxin (0.5µM). A strictly identical protocol was followed to assess the effect of *FBXW7* **(b)**, *GSK3β* **(c)**, *UBE2L3* **(d)**, *HUWE1* **(e)**, *PSME3* **(f)**, *TBL1XR1* **(g)**, *BUB3* **(h)**, *CBL*, *BRCA1*, *UBE4A* **(i)**, *UBE4B*, *MDM2*, *STUB1* **(j)**, and of *TRIM21* and *TRIM33* **(k)** knockdowns on REV-ERBα stability. Normalized data are plotted as mean+/-SEM (n=3-6) and compared using a one-way ANOVA test, followed by a Tukey's multiple comparison test. All measurements were from distinct samples.

Extended data Fig. 10. Screening E2/E3 ligases potentially involved in digoxin-induced REV-ERBα degradation. (a) REV-ERBα protein level in AC16 cells transfected either with scrambled siRNA (Scr siRNA) or *SIAH2* siRNA and treated with vehicle or digoxin (0.5µM). A strictly identical protocol was followed to assess the effect of *FBXW7* **(b)**, *GSK3β* **(c)**, *UBE2L3* **(d)**, *HUWE1* **(e)**, *PSME3* **(f)**, *TBL1XR1* **(g)**, *BUB3* **(h)**, *CBL*, *BRCA1*, *UBE4A* **(i)**, *UBE4B*, *MDM2*, *STUB1* **(j)**, and of *TRIM21* and *TRIM33* **(k)** knockdowns on REV-ERBα stability.

Supplemental Dataset 1. Gene expression profiling in ZT0 vs ZT12 mouse hearts. Mouse hearts were collected at ZT0 or ZT12 (n=7 per group) and RNAs were extracted and quantified by Affymetrix arrays. Results are expressed as fold change and corrected p values are indicated (fold-change > 1.2 with an FDR < 0.05, after a moderated t-test followed by a Benjamini-Hochberg multiple testing correction). For the sake of clarity, only protein-encoding genes are indicated.

Supplemental Dataset 2. Gene expression profiling in Nr1d1$^{+/+}$ vs Nr1d1$^{-/-}$ (ZT12) mouse hearts. Mouse hearts were collected at ZT12 (n=7 per group) from Nr1d1$^{+/+}$ vs Nr1d1$^{-/-}$ mice and RNAs were extracted and quantified by Affymetrix arrays. Results are expressed as fold change and corrected p

values are indicated (fold-change > 1.2 with an FDR < 0.05, after a moderated t-test followed by a Benjamini-Hochberg multiple testing correction). For the sake of clarity, only protein-encoding genes are indicated.

Supplemental Dataset 3. Transcriptomic alterations in digoxin-treated AC16 cells. AC16 cells were treated after synchronization by low (0.5µM) or high (5µM) digoxin concentrations (n=3). mRNA levels were quantified by Affymetrix arrays. Results are expressed as fold change and corrected p values are indicated (fold-change > 1.2 with an FDR < 0.05, after a moderated t-test followed by a Benjamini-Hochberg multiple testing correction). For the sake of clarity, only protein-encoding genes are indicated.

Supplemental Dataset 4. Transcriptomic alterations in digoxin-treated mice. Mice were injected at ZT5 and hearts were collected at ZT9 (n=3-5). After RNA extraction, gene expression was assayed and expressed as described in Supplementary Dataset 1 (fold-change > 1.2 with an FDR < 0.05, after a moderated t-test followed by a Benjamini-Hochberg multiple testing correction). For the sake of clarity, only protein-encoding genes are indicated.

Supplementary Dataset 5. Transcriptomic alterations common to mouse heart and human AC16 cells. Data from Supplementary Datasets 1 and 2 were compared and common genes to both lists are indicated.

Supplementary Dataset 6. REV-ERBα RIME data. REV-ERBα was pulled down from AC16 and HepG2 cells and associated proteins were identified by LC-MS/MS (n=1 for HepG2 and n=2 for U2OS). The list of common REV-ERBα interactants is shown, with selected interactants related to UPS indicated in bold. The threshold for significant interaction was arbitrarily set to 5 detected peptides to select a testable set of interactants.

1145

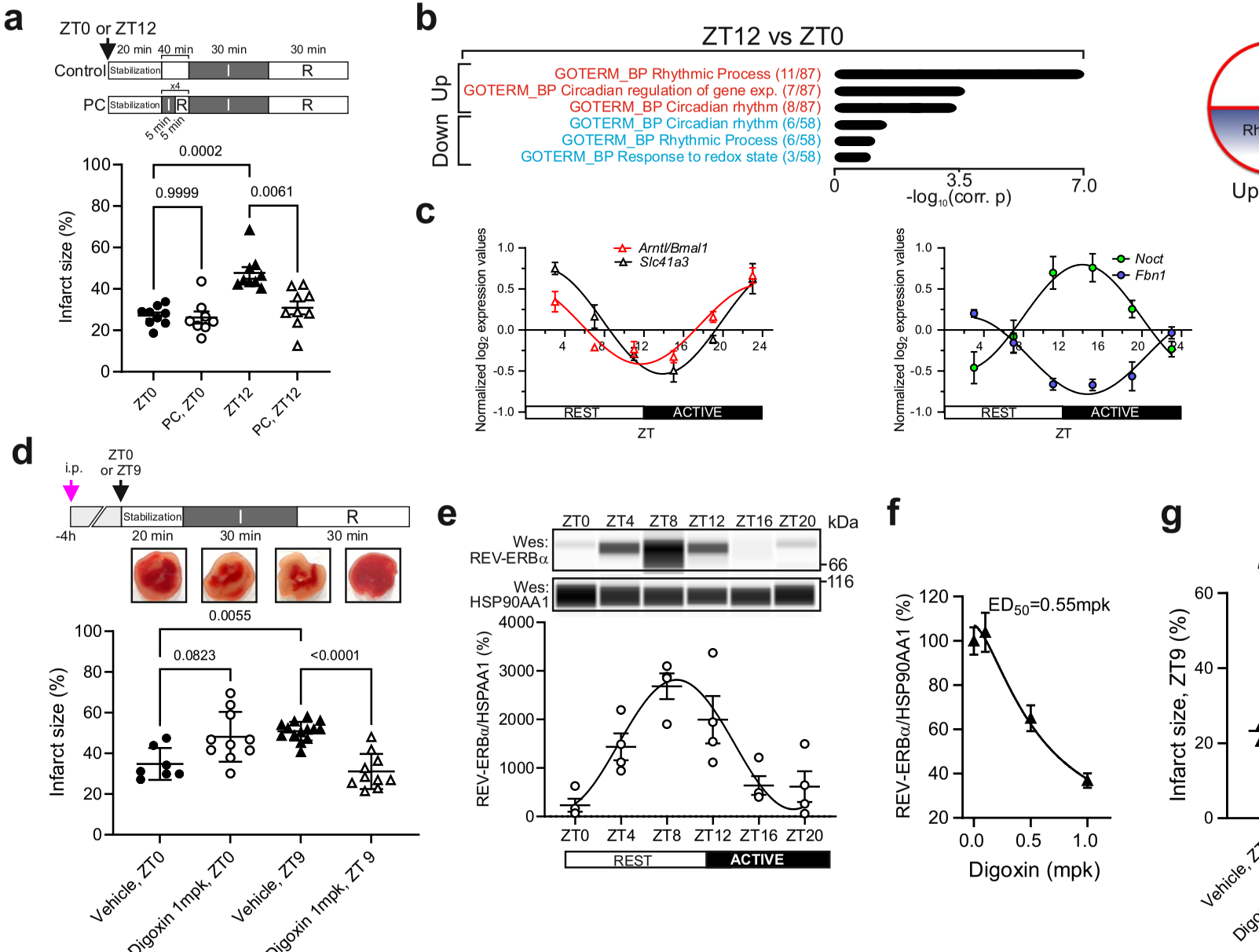

Vinod et al. - FIGURE 1

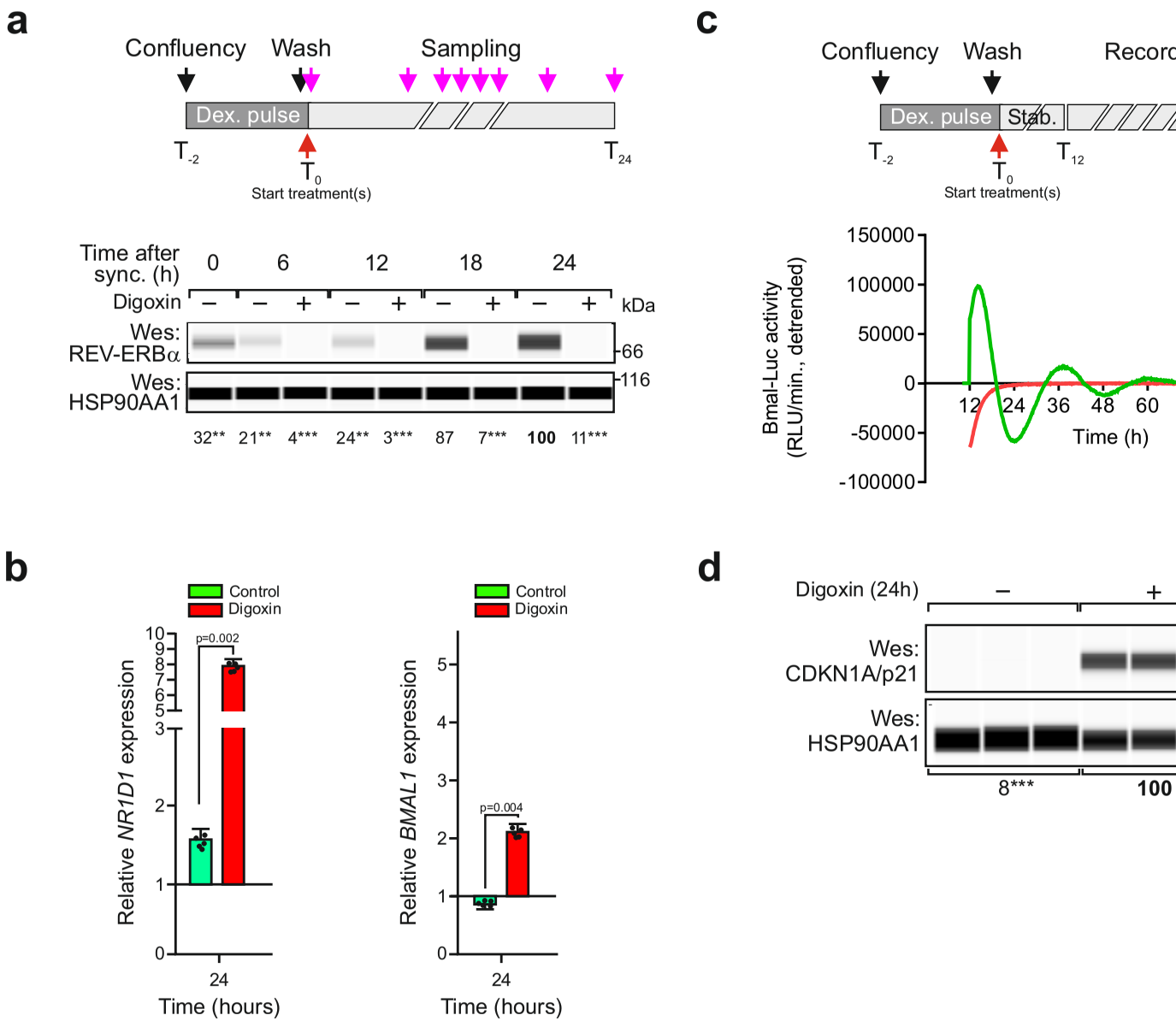

Vinod et al. - FIGURE 2

Human primary cardiomyocytes

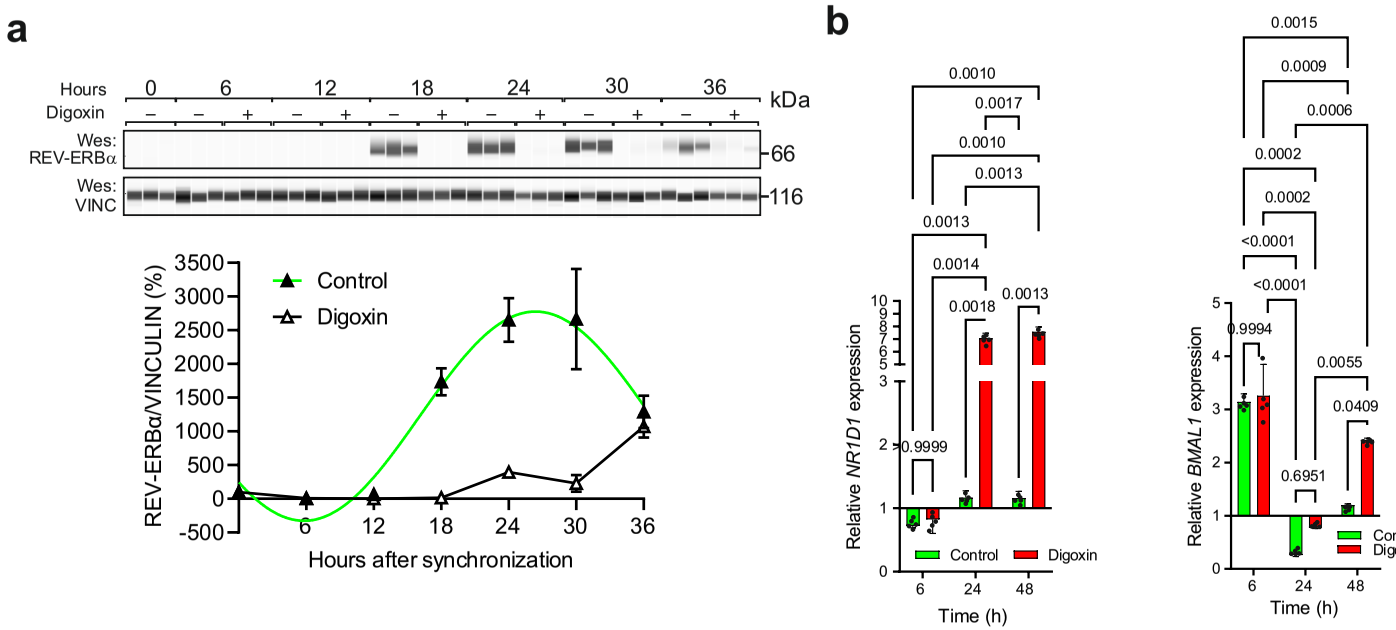

Vinod et al. - FIGURE 3

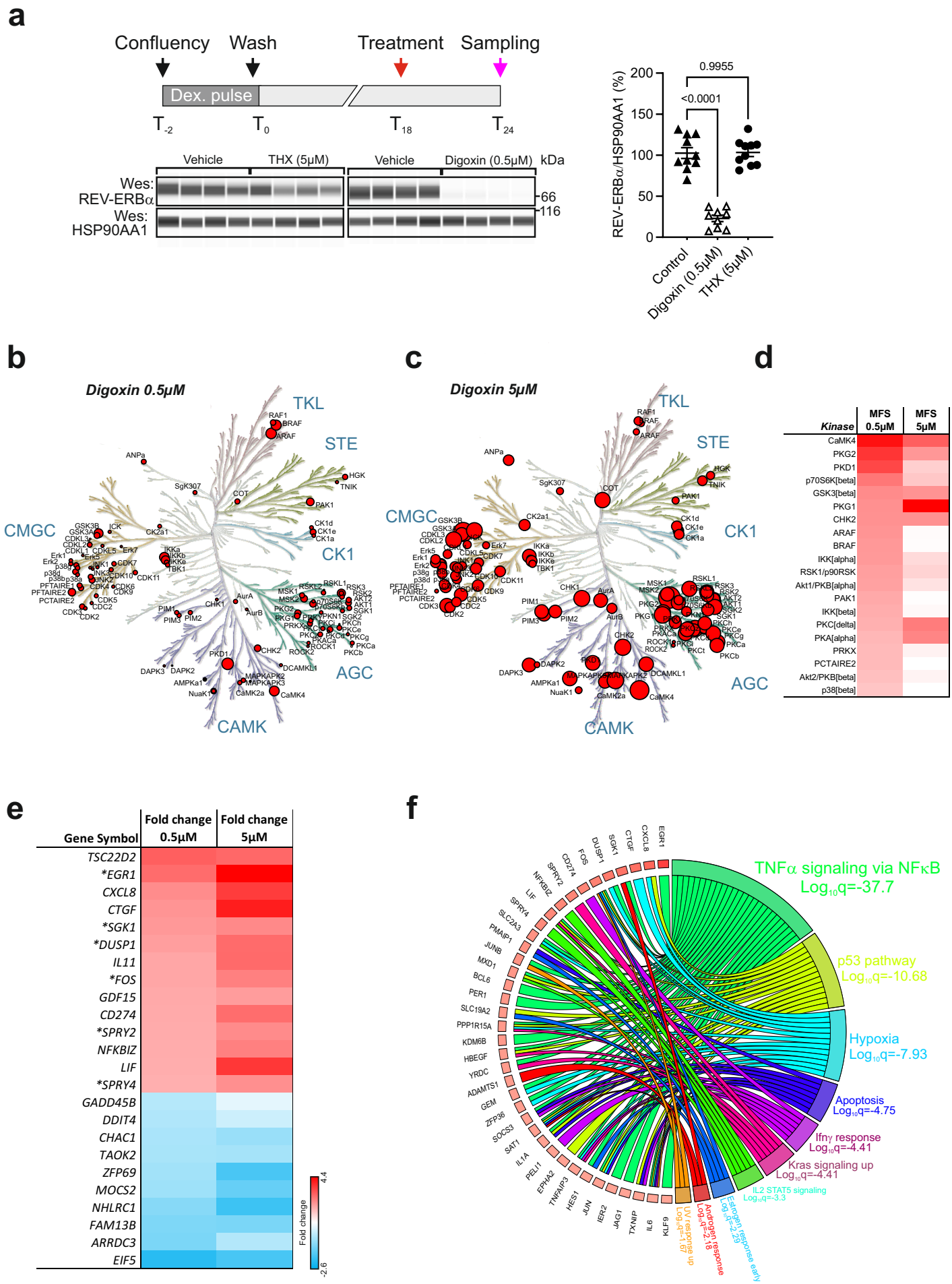

Vinod et al. - FIGURE 4

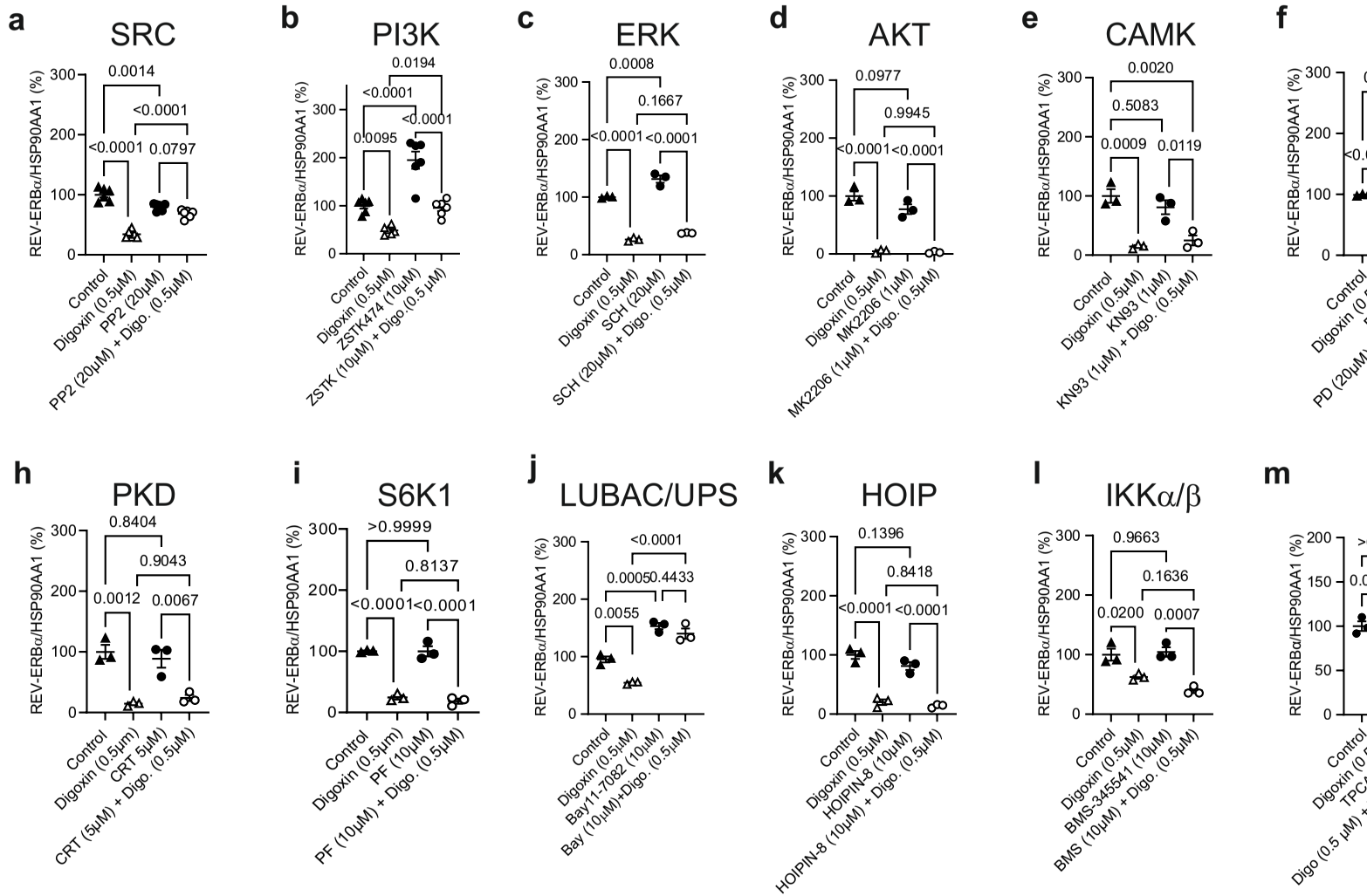

Vinod et al. - FIGURE 5

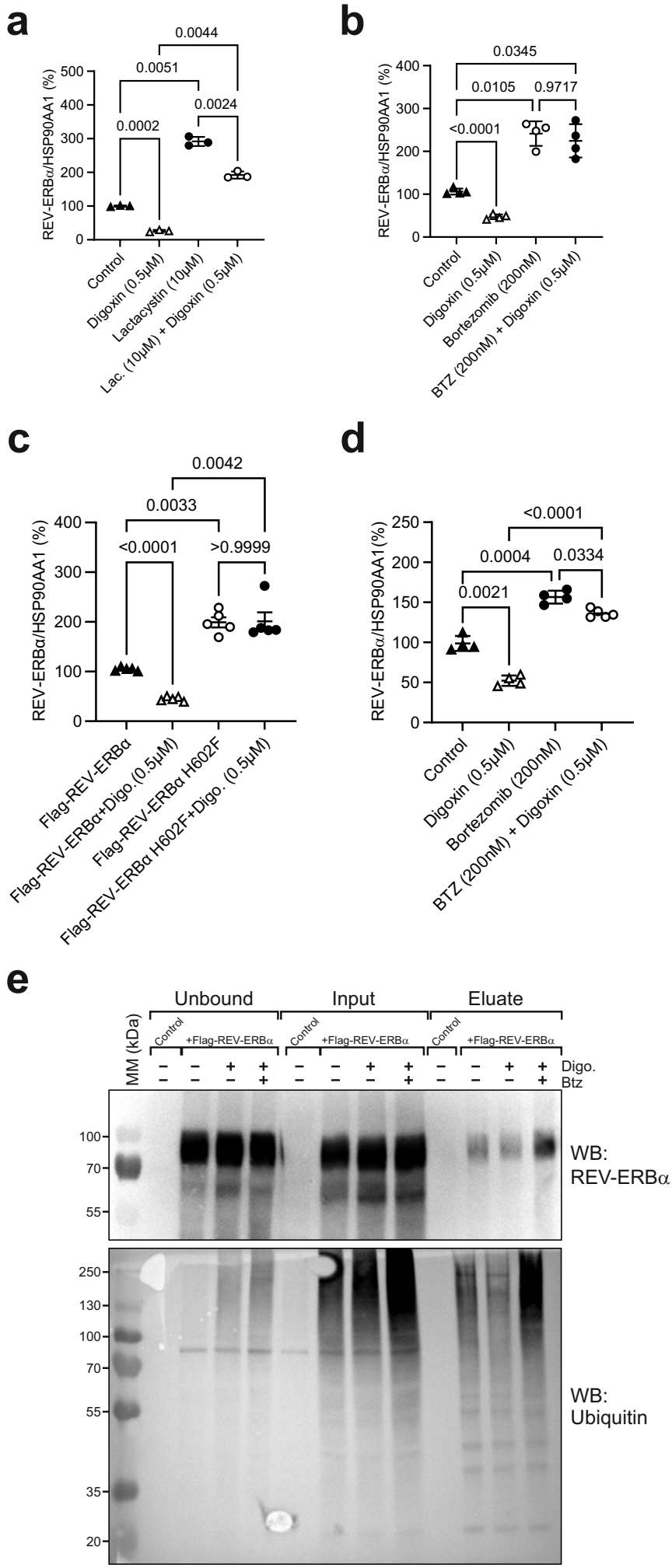

Vinod et al. - FIGURE 6

a

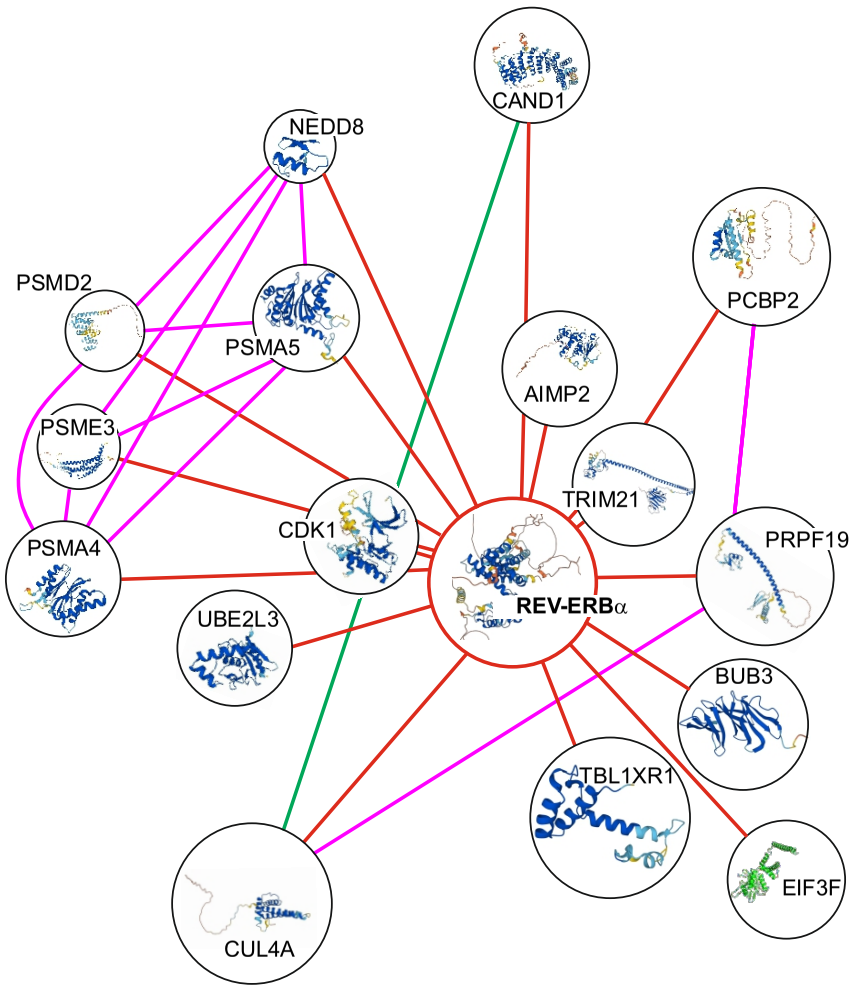

b

	REV-ERBα interactants	IP	RS
NR	NEDD8	■	
	PSMD2		
	PSMA5		
	PSME3		■
	PSMA4		
	UBE2L3		■
	CUL4A		
	CAND1		
	TBL1XR1		■
	CDK1	■	
	AIMP2		
	TRIM21		
	EIF3F		
	BUB3		■
	PRPF19		
	PCBP2		
E3L	SIAH2		■
	FBXW7		■
	GSK3β	■	■
	CBL		■
	BRCA1		■
	UBE4A		■
	UBE4B		■
	MDM2		■
	STUB1		■
	TRIM33		■
	HUWE1		■
	PSMB5	■	

Vinod et al. - FIGURE 7

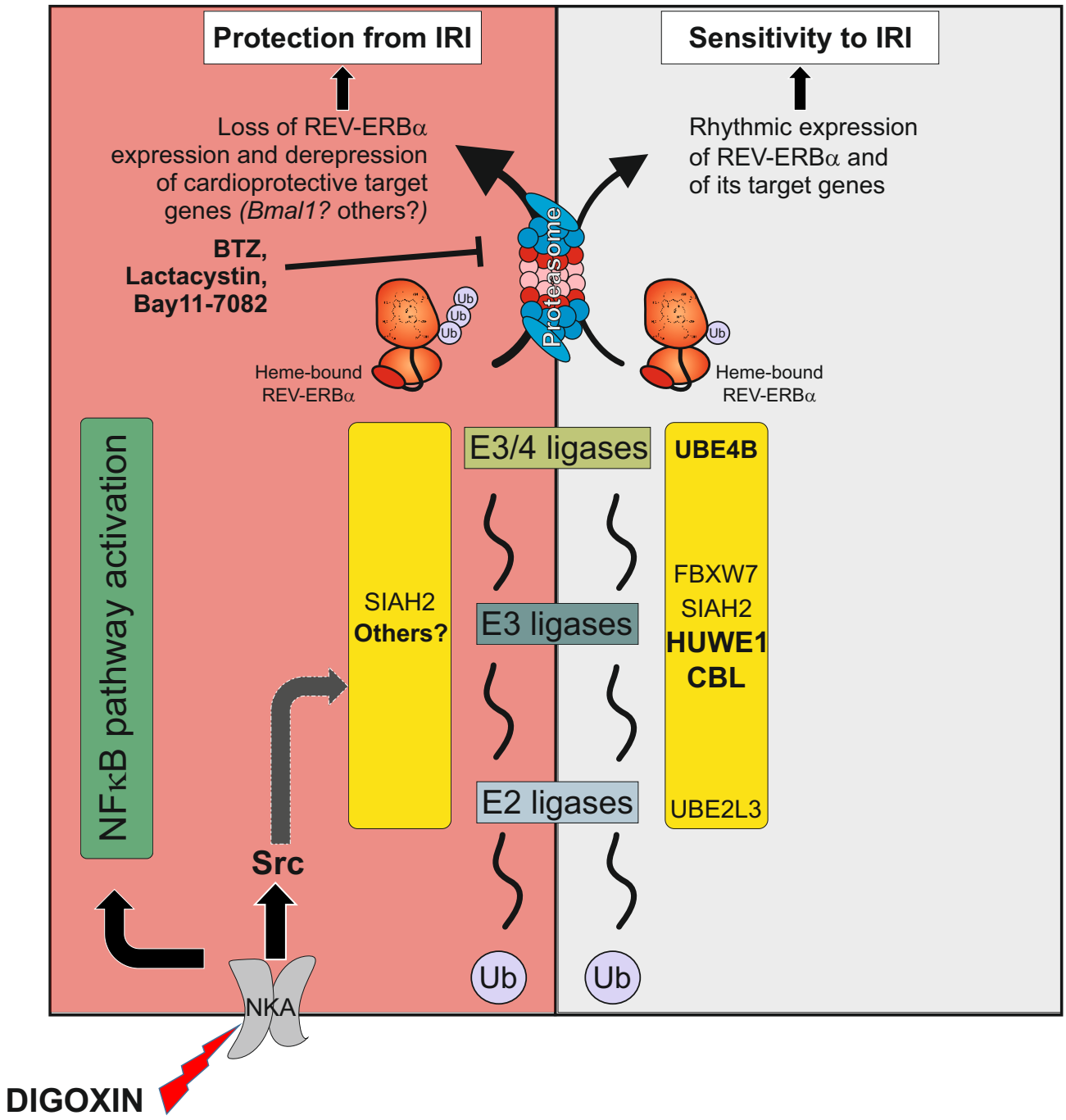

Vinod et al. - FIGURE 8

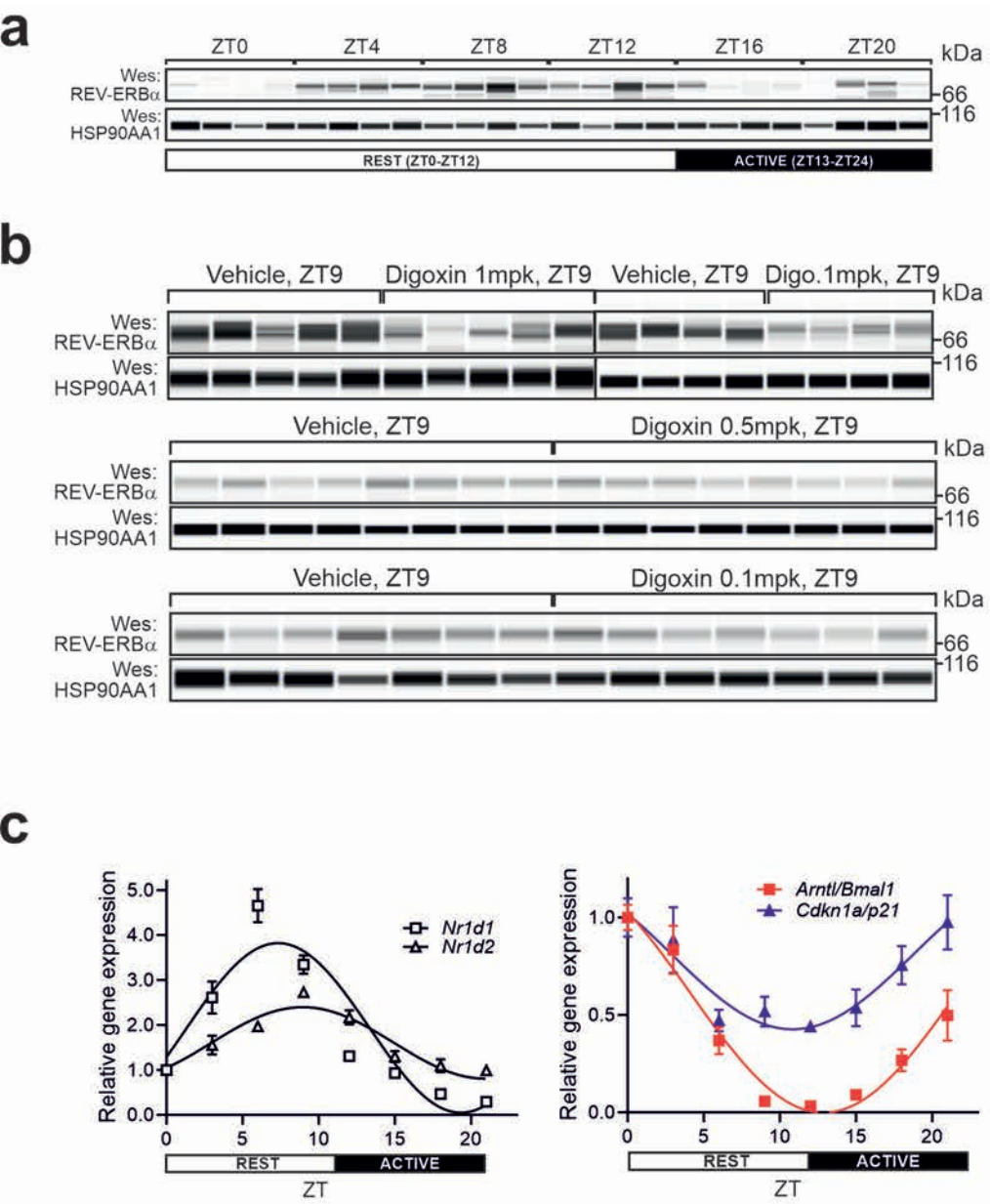

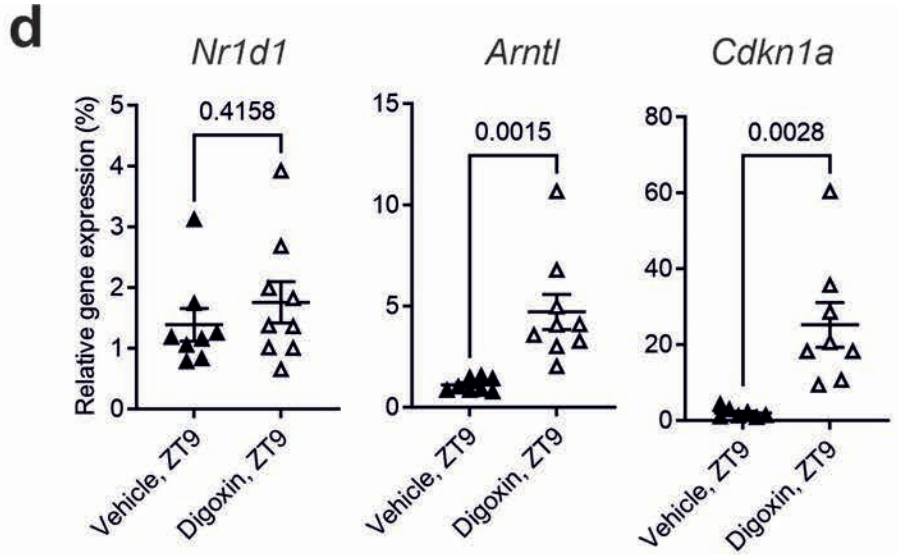

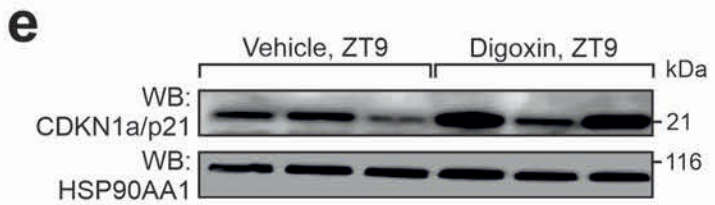

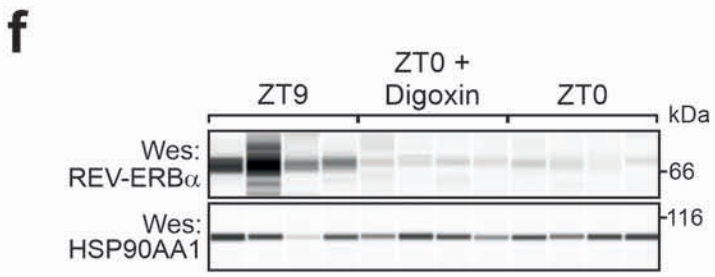

Vinod et al. - Ext. Figure 1

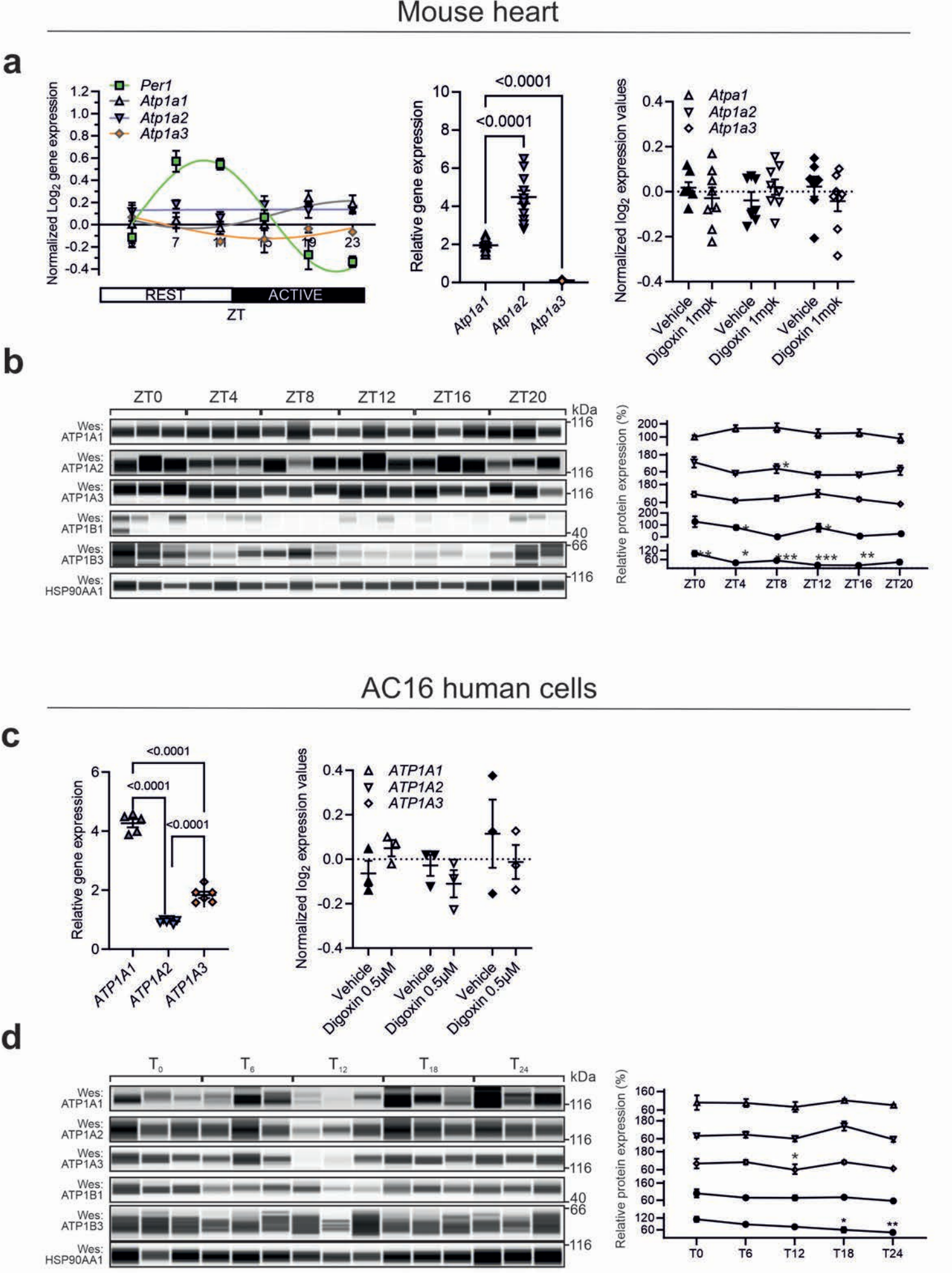

Vinod et al. - Ext. Figure 2

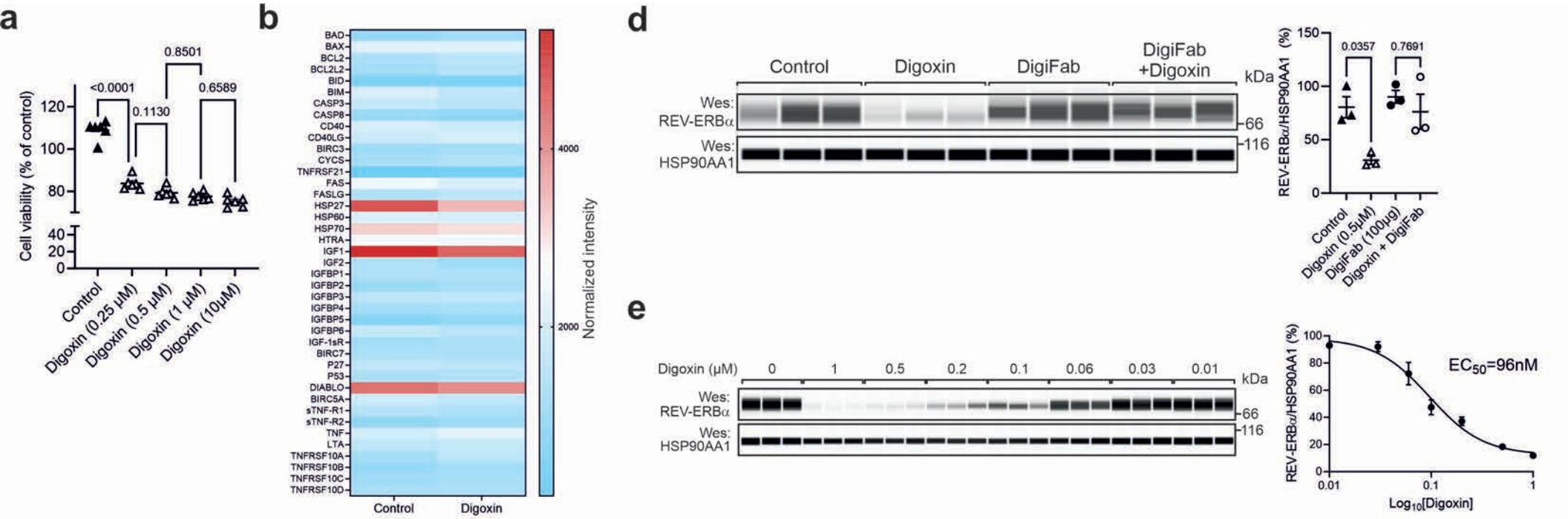

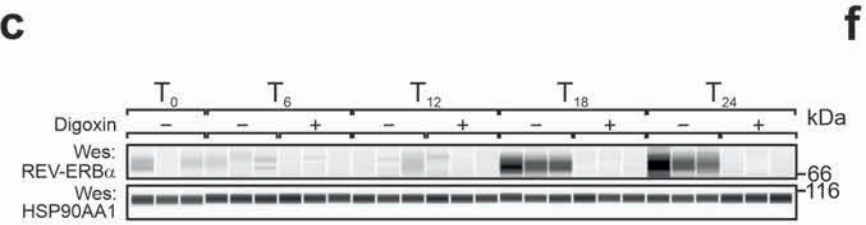

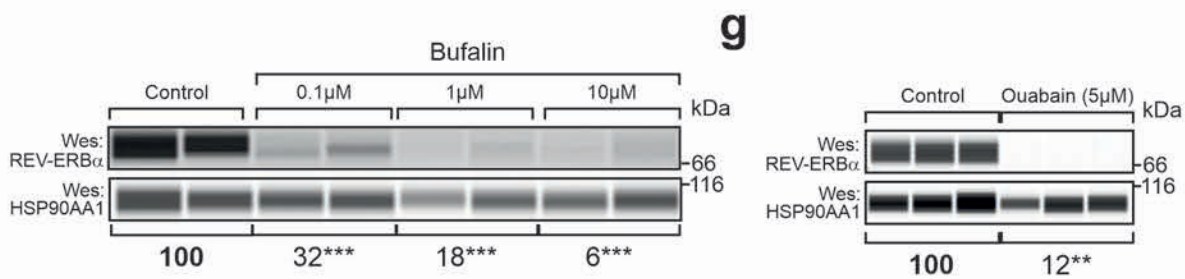

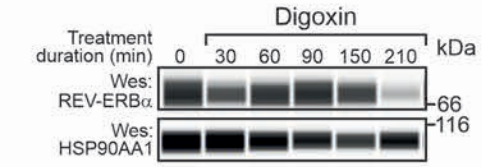

Vinod et al. - Ext. Figure 3

Human osteosarcoma U2OS cells

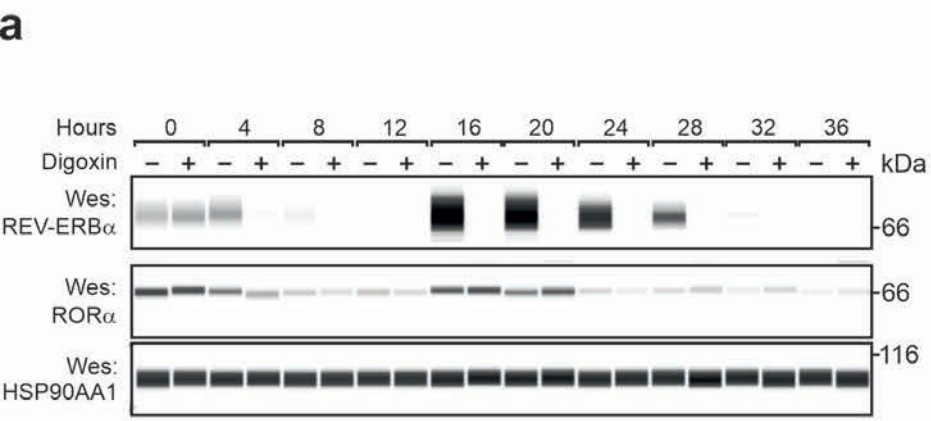

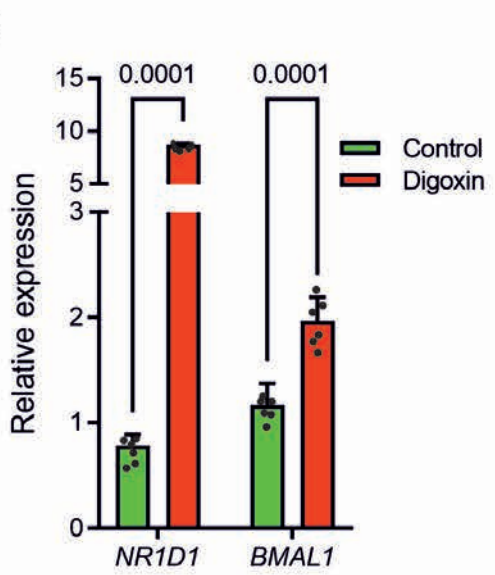

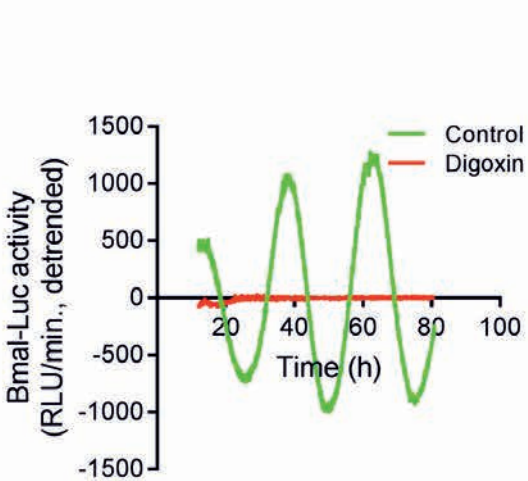

Vinod et al. - Ext Figure 4

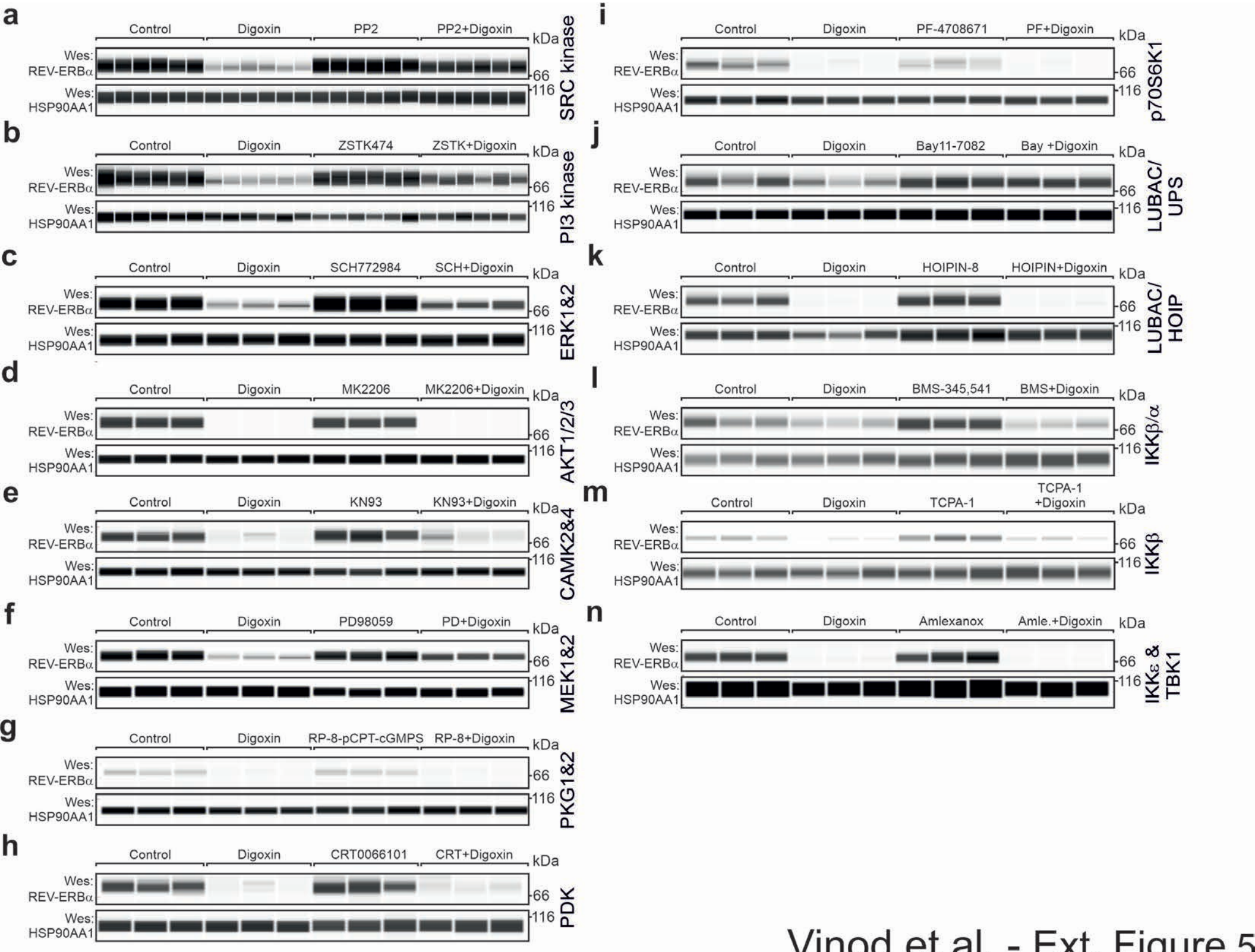

Vinod et al. - Ext. Figure 5

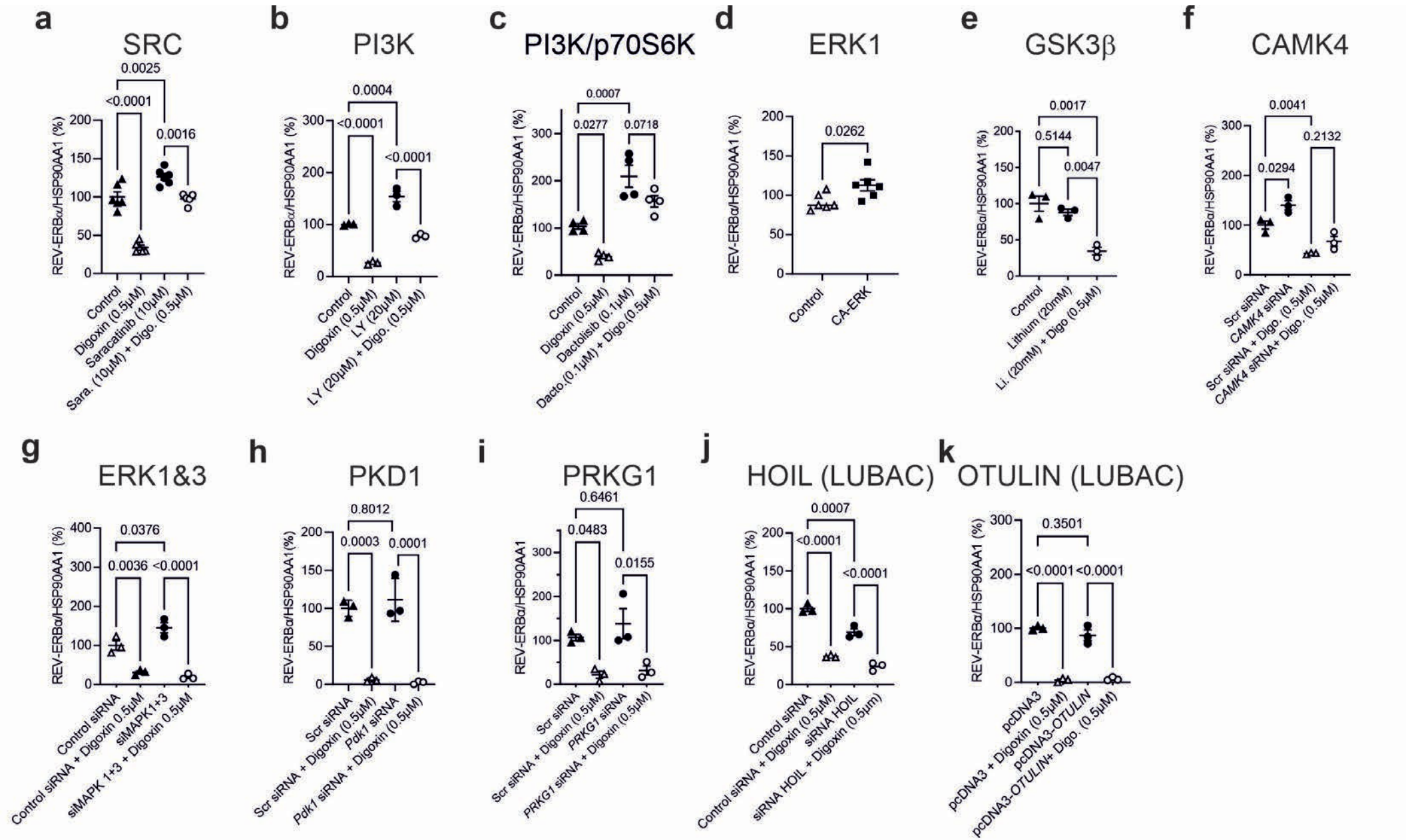

Vinod et al. - Ext. Figure 6

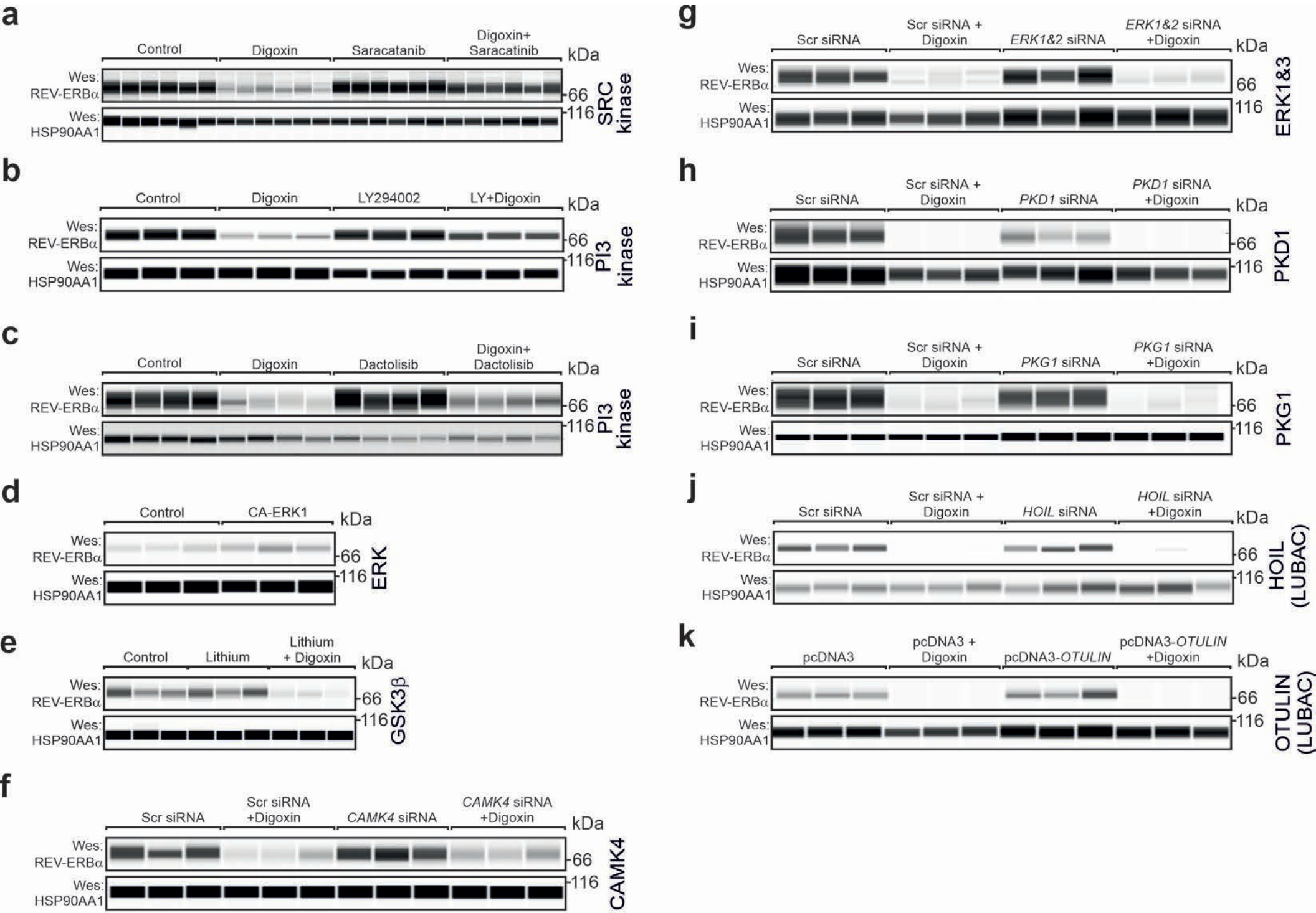

Vinod et al. - Ext Figure 7

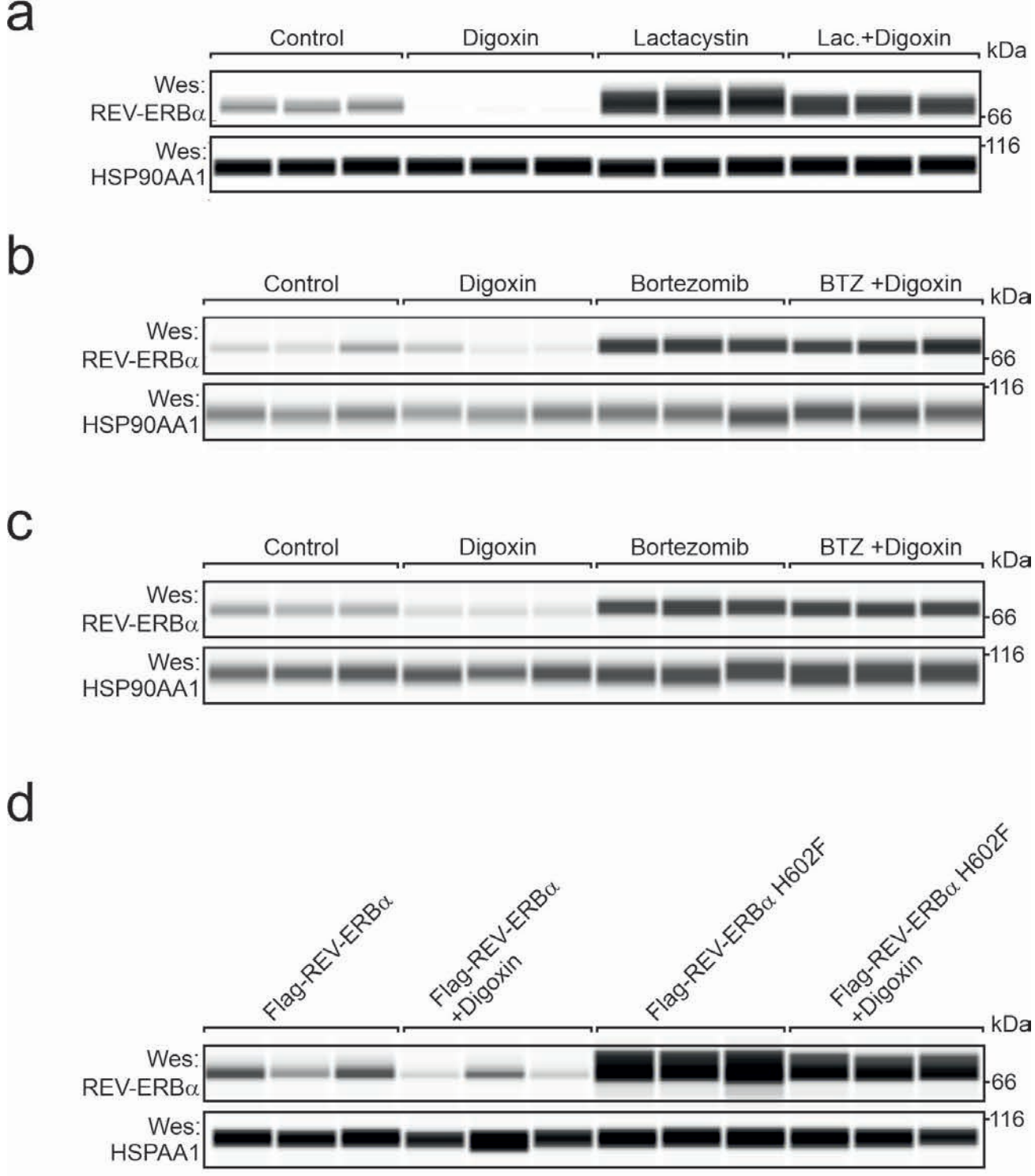

Vinod et al. - Ext. Figure 8

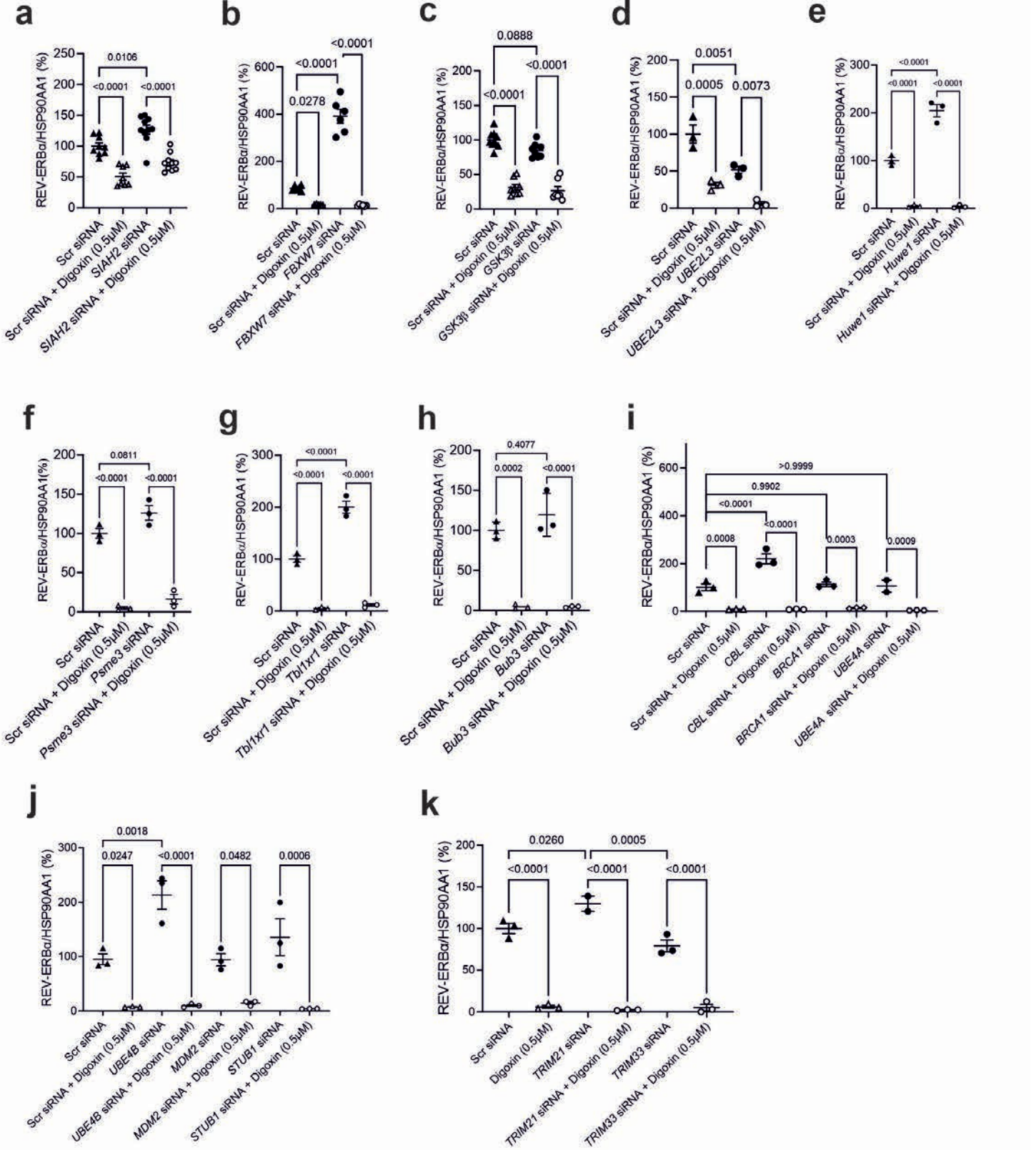
a
REV-ERBα/HSP90AA1 (%)
0.0106
<0.0001
<0.0001
Scr siRNA
Scr siRNA + Digoxin (0.5μM)
SIAH2 siRNA
SIAH2 siRNA + Digoxin (0.5μM)
b
REV-ERBα/HSP90AA1 (%)
<0.0001
<0.0001
0.0278
Scr siRNA
Scr siRNA + Digoxin (0.5μM)
FBXW7 siRNA
FBXW7 siRNA + Digoxin (0.5μM)
c
REV-ERBα/HSP90AA1 (%)
0.0888
<0.0001
<0.0001
Scr siRNA
Scr siRNA + Digoxin (0.5μM)
GSK3β siRNA
GSK3β siRNA+ Digoxin (0.5μM)
d
REV-ERBα/HSP90AA1 (%)
0.0051
0.0005
0.0073
Scr siRNA
Scr siRNA + Digoxin (0.5μM)
UBE2L3 siRNA
UBE2L3 siRNA + Digoxin (0.5μM)
e
REV-ERBα/HSP90AA1 (%)
<0.0001
<0.0001
<0.0001
Scr siRNA
Scr siRNA + Digoxin (0.5μM)
Huwe1 siRNA
Huwe1 siRNA + Digoxin (0.5μM)
f
REV-ERBα/HSP90AA1(%)
0.0811
<0.0001
<0.0001
Scr siRNA
Scr siRNA + Digoxin (0.5μM)
Psme3 siRNA
Psme3 siRNA + Digoxin (0.5μM)
g
REV-ERBα/HSP90AA1 (%)
<0.0001
<0.0001
<0.0001
Scr siRNA
Scr siRNA + Digoxin (0.5μM)
Tbl1xr1 siRNA
Tbl1xr1 siRNA + Digoxin (0.5μM)
h
REV-ERBα/HSP90AA1 (%)
0.4077
0.0002
<0.0001
Scr siRNA
Scr siRNA + Digoxin (0.5μM)
Bub3 siRNA
Bub3 siRNA + Digoxin (0.5μM)
i
REV-ERBα/HSP90AA1 (%)
>0.9999
0.9902
<0.0001
<0.0001
0.0008
0.0003
0.0009
Scr siRNA
Scr siRNA + Digoxin (0.5μM)
CBL siRNA
CBL siRNA + Digoxin (0.5μM)
BRCA1 siRNA
BRCA1 siRNA + Digoxin (0.5μM)
UBE4A siRNA
UBE4A siRNA + Digoxin (0.5μM)
j
REV-ERBα/HSP90AA1 (%)
0.0018
0.0247
<0.0001
0.0482
0.0006
Scr siRNA
Scr siRNA + Digoxin (0.5μM)
UBE4B siRNA
UBE4B siRNA + Digoxin (0.5μM)
MDM2 siRNA
MDM2 siRNA + Digoxin (0.5μM)
STUB1 siRNA
STUB1 siRNA + Digoxin (0.5μM)
k
REV-ERBα/HSP90AA1 (%)
0.0260
0.0005
<0.0001
<0.0001
<0.0001
Scr siRNA
Digoxin (0.5μM)
TRIM21 siRNA
TRIM21 siRNA + Digoxin (0.5μM)
TRIM33 siRNA
TRIM33 siRNA + Digoxin (0.5μM)

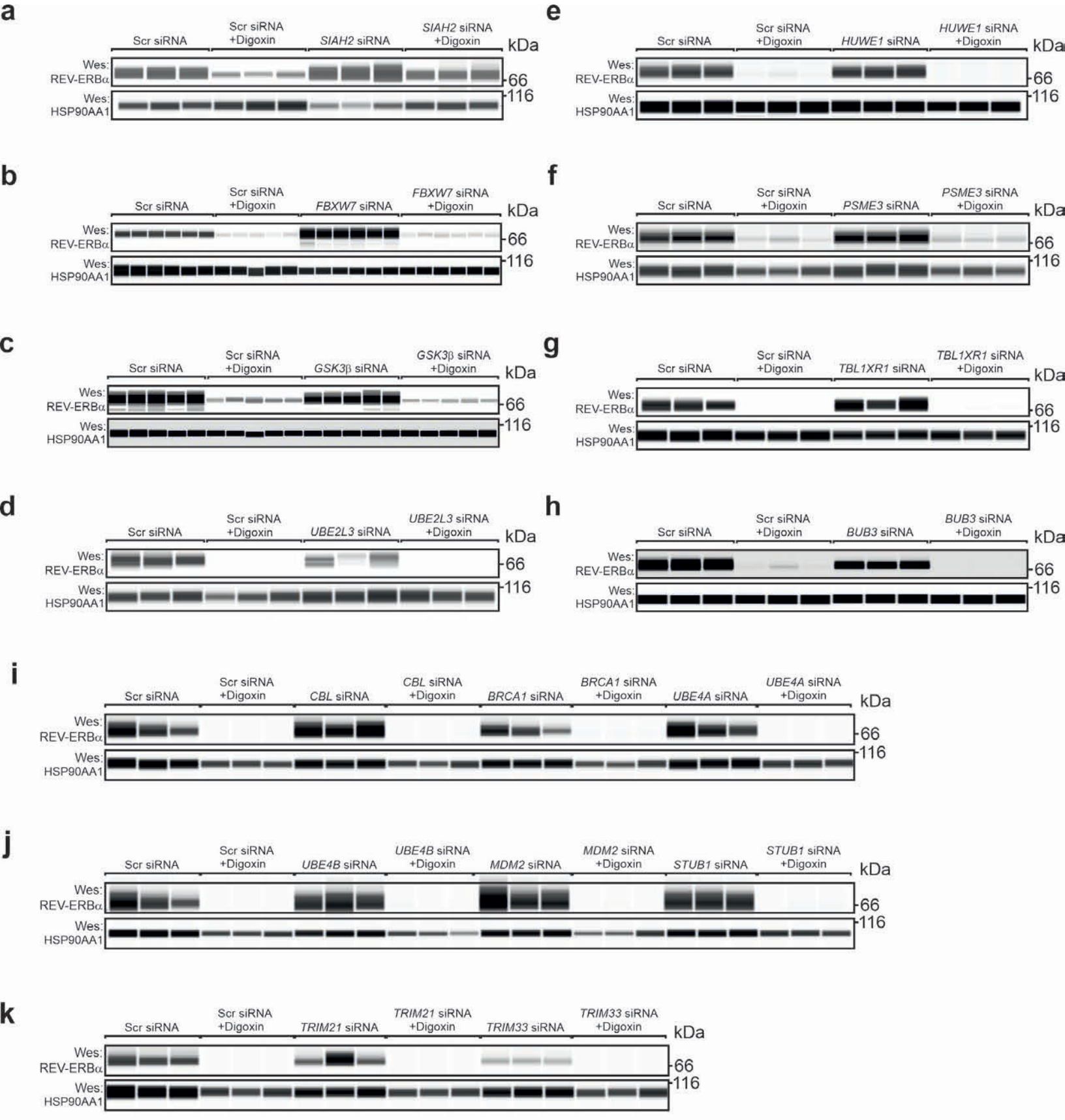

Vinod et al. - Ext Figure 10